The plasmablast response to SARS-CoV-2 mRNA vaccination is dominated by non-neutralizing antibodies and targets both the NTD and the RBD

Fatima Amanat[1,2], Mahima Thapa[3], Tinting Lei[3], Shaza M. Sayed Ahmed[3], Daniel C. Adelsberg[1], Juan Manuel Carreno[1], Shirin Strohmeier[1], Aaron J. Schmitz[3], Sarah Zafar[1], Julian Q Zhou[4], Willemijn Rijnink[1], Hala Alshammary[1], Nicholas Borcherding[3], Ana Gonzalez Reiche[5], Komal Srivastava, Emilia Mia Sordillo[6], Harm van Bakel[5,7], The Personalized Virology Initiative[#], Jackson S. Turner[3], Goran Bajic[1], Viviana Simon[1,8,9], Ali H. Ellebedy[3,10,11], Florian Krammer[1]

Affiliations

[1]*Department of Microbiology, Icahn School of Medicine at Mount Sinai, New York, NY 10029, USA*
[2]*Graduate School of Biomedical Sciences, Icahn School of Medicine at Mount Sinai, New York, NY 10029, USA*
[3]*Department of Pathology & Immunology, Washington University School of Medicine, St. Louis, MO, 63110, USA*
[4]*AbCellera Biologics Inc., Vancouver, BC V5Y 0A1, Canada*
[5]*Department of Genetics and Genomic Sciences, Icahn School of Medicine at Mount Sinai, New York, NY 10029, USA*
[6]*Department of Pathology, Molecular and Cell Based Medicine, Icahn School of Medicine at Mount Sinai, New York, NY 10029, USA*
[7]Icahn Institute for Data Science and Genomic Technology, Icahn School of Medicine at Mount Sinai, New York, NY 10029, USA
[8]*Division of Infectious Diseases, Department of Medicine, Icahn School of Medicine at Mount Sinai, New York, NY 10029, USA*
[9]*The Global Health and Emerging Pathogens Institute, Icahn School of Medicine at Mount Sinai, New York, NY 10029, USA*
[10]*Andrew M. and Jane M. Bursky Center for Human Immunology and Immunotherapy Programs, Washington University School of Medicine, Saint Louis, MO 63110, USA*
[11]*Center for Vaccines and Immunity to Microbial Pathogens, Washington University School of Medicine, Saint Louis, MO 63110, USA*

[#]Personalized Virology Initiative (PVI) Study group/Consortium (in alphabetical order): Dr. Bulbul Ahmed, Dr. Deena Altman, Angela Amoako, Mahmoud Awawda, Katherine Beach, Carolina Bermúdez-González, Rachel Chernet, Lily Eaker, Shelcie Fabre, Emily. D. Ferreri, Daniel Floda, Charles Gleason, Dr. Giulio Kleiner, Dr. Denise Jurczyszak, Julia Matthews, Wanni Mendez, Dr. Lubbertus CF Mulder, Jose Polanco, Kayla Russo, Ashley Salimbangon, Dr. Miti Saksena, Amber S. Shin , Levy Sominsky, Sayahi Suthakaran, Dr. Ania Wajnberg

Corresponding authors
Goran Bajic, goran.bajic@mssm.edu
Viviana Simon, viviana.simon@mssm.edu
Ali H. Ellebedy, ellebedy@wustl.edu
Florian Krammer, florian.krammer@mssm.edu

Summary

In this study we profiled vaccine-induced polyclonal antibodies as well as plasmablast derived mAbs from individuals who received SARS-CoV-2 spike mRNA vaccine. Polyclonal antibody responses in vaccinees were robust and comparable to or exceeded those seen after natural infection. However, the ratio of binding to neutralizing antibodies after vaccination was greater than that after natural infection and, at the monoclonal level, we found that the majority of vaccine-induced antibodies did not have neutralizing activity. We also found a co-dominance of mAbs targeting the NTD and RBD of SARS-CoV-2 spike and an original antigenic-sin like backboost to seasonal human coronaviruses OC43 and HKU1. Neutralizing activity of NTD mAbs but not RBD mAbs against a clinical viral isolate carrying E484K as well as extensive changes in the NTD was abolished, suggesting that a proportion of vaccine induced RBD binding antibodies may provide substantial protection against viral variants carrying single E484K RBD mutations.

Introduction

Understanding of the innate and adaptive immune responses to severe acute respiratory syndrome coronavirus 2 (SARS-CoV-2) has progressed rapidly since the beginning of the coronavirus disease 2019 (COVID-19) pandemic (Carvalho et al., 2021). Polyclonal antibody responses against the spike protein of the virus in serum, and to a lesser degree also at mucosal surfaces, have been well characterized with respect to their kinetics, binding capacity and functionality (Grandjean et al., 2020; Isho et al., 2020; Iyer et al., 2020; Ripperger et al., 2020; Seow et al., 2020; Wajnberg et al., 2020). Similarly, encouraging data have been published on both the plasmablast response and the memory B-cell response induced by SARS-CoV-2 infection (Dan et al., 2021; Gaebler et al., 2020; Guthmiller et al., 2021; Huang et al., 2021; Robbiani et al., 2020; Rodda et al., 2021; Wilson et al., 2020). The immune responses to SARS-CoV-2 vaccination, including to mRNA-based vaccines, are less well studied since these vaccines have only become available in the last months of 2020 (Baden et al., 2020; Polack et al., 2020). However, understanding vaccine-induced immunity is of high importance given the goal to achieve immunity for most people through vaccination, rather than as a consequence of infection.

The receptor binding domain (RBD) of the SARS-CoV-2 spike is an important target for serological and B-cell studies because it directly interacts with the cellular receptor angiotensin converting enzyme 2 (ACE2) mediating host cell entry (Letko et al., 2020; Wrapp et al., 2020). Antibodies binding to the RBD can potently block attachment of the virus to ACE2 and thereby neutralize the virus (Barnes et al., 2020). As a consequence, RBD-based vaccines are in development in addition to full length spike-based vaccines (Krammer, 2020). Analyses of the B-cell responses to the spike generally focus on the RBD and on cells sorted with RBD baits introducing an inherent bias by omitting non-RBD targets (Cao et al., 2020; Gaebler *et al.*, 2020; Robbiani *et al.*, 2020; Weisblum et al., 2020). This is also true for B cells and monoclonal antibodies (mAbs) isolated from vaccinated individuals (Wang et al., 2021). However, other epitopes within the spike protein, notably the N-terminal domain (NTD) but also S2, do harbor neutralizing epitopes (Chi et al., 2020; Liu et al., 2020; McCallum et al., 2021b; Song et al., 2020). In fact, the NTD is heavily mutated in the three most prominent variants of concern (VOCs, B.1.1.7, B.1.351 and P.1 (Davies et al., 2021; Faria et al., 2021; Tegally et al., 2020)). Here, we studied the unbiased plasmablast response to SARS-CoV-2 mRNA-based vaccination and report several new findings. First, we document that RBD and NTD co-dominate as B-cell targets on the viral spike protein, highlighting the importance of the NTD. We also report the first vaccine-induced NTD mAbs. In addition, we show that the majority of mAbs isolated are non-neutralizing, which is reflective of the higher binding to neutralization ratios found in serum after vaccination compared to natural infection. Finally, data from plasmablasts suggest that, at least, some of the vaccine-induced response is biased by pre-existing immunity to human β-coronaviruses.

Results

The polyclonal antibody response to mRNA vaccination exceeds titers seen in convalescent individuals but is characterized by a high ratio of non-neutralizing antibodies

In late 2020, six adult participants of an ongoing observational study received mRNA-based SARS-CoV-2 vaccines (**Suppl. Table 1**). Blood from these individuals (termed V1-V6) was collected at several time points including before vaccination (for 4/6), after the first vaccination and at several time points after the second vaccination. We examined their immune responses to recombinant spike protein and RBD in enzyme-linked immunosorbent assays (ELISA), in comparison to those of 30 COVID-19 survivors (**Figure 1A and 1B, Suppl. Table 1**). The sera from convalescent individuals were selected based on their anti-spike titers and grouped into three groups (low +: n=8; moderate ++: n=11; and high +++: n=11, based on the antibody titer measured in the Mount Sinai's CLIA laboratory (Wajnberg *et al.*, 2020)), in order to facilitate identifying different features that may track with the strength of the antibody response. Five out of six vaccinees produced anti-spike and anti-RBD responses that were, at the peak, markedly higher than responses observed even in the high titer convalescent group while one vaccinee (V4) produced titers comparable to the high titer group. Notably, the antibody response peaked one week after the second vaccine dose, followed by a decline in titers over the following weeks as expected from an antibody response to vaccination. Interestingly, anti-RBD antibody titers seemed to decline faster than anti-spike antibody titers, which appeared to be more stable over time. We also measured neutralizing antibody titers using authentic SARS-CoV-2 and found a similar trend with all vaccinees displaying high titers, even though V4 responded with delayed kinetics (**Figure 1C**). Importantly, although at the peak response, the vaccine group mounted neutralization titers that fell in the upper range for the high convalescent group, they did not exceed that group markedly. This finding prompted us to calculate the proportions of spike binding to neutralizing antibodies. For the convalescent group, we found that individuals with lower titers had a higher proportion of binding to neutralizing antibodies than high responding convalescent individuals (**Figure 1D**). When determined at the time of peak response, the vaccinees had the highest proportion of binding to neutralizing antibody titers, indicating an immune response focused on non-neutralizing antibodies or an induction of less potent neutralizing antibodies in general (or both). These proportions remained stable over time with the ratio of binding to neutralizing antibodies in vaccinated individuals being significantly higher than those observed for any of the three convalescent groups ($p = 0.0004$, 0.0002 and 0.0041 for the three groups respectively; **Suppl. Figure 1**). We also investigated the spike binding to RBD binding ratio and found no difference to convalescent individuals except a general trend towards proportionally less RBD binding over time in the vaccinees (**Suppl. Figure 1**).

mRNA vaccination induces a modest but measurable immune response to seasonal β-coronavirus spike proteins

It has been reported that SARS-CoV-2 infection induces an original antigenic sin-type immune response against human coronaviruses (hCoVs) to which the majority of the human population has pre-existing immunity (Aydillo et al., 2020; Song *et al.*, 2020). Here, we explored whether this phenomenon is also induced by SARS-CoV-2 mRNA vaccination. Antibody titers in four vaccinees against spike protein from α-coronaviruses 229E and NL63 were detectable at the pre-vaccination time point, but did not increase substantially post-vaccination (**Figure 1E-F**; for V5 and V6 no pre-vaccination serum was available). However, titers against the spike proteins of β-coronaviruses OC43 and HKU1 increased substantially in these four vaccinees after vaccination (**Figure 1G-H)**. Thus, vaccination with mRNA SARS-

140 CoV-2 spike also boosts immune responses against seasonal β-coronavirus spike proteins in a manner
141 reminiscent of that reported for natural infection with SARS-CoV-2.

142 **Plasmablast response to SARS-CoV-2 mRNA vaccination targets both the RBD and the NTD**

143 In order to characterize the B-cell response to vaccination in an unbiased manner, plasmablasts
144 were single-cell sorted from blood specimens obtained from three individuals (V3, V5 and V6) one week
145 after the booster immunization (**Suppl. Figure 2**). All mAbs were generated from single-cell sorted
146 plasmablasts and probed for binding to recombinant SARS-CoV-2 spike protein. Twenty-one (40 mAbs
147 were screened, with 28 being clonally unique, **Suppl. Table 2**) spike-reactive mAbs were isolated from V3,
148 six (82 screened, 20 unique) from V5 and fifteen (84 screened, 24 unique) from V6 (**Figure 2A**). Using
149 recombinant spike, RBD, NTD and S2 proteins, we mapped the domains to which these mAbs bind.
150 Interestingly, only a minority of these antibodies recognized RBD (24% for V3, 47% for V6 and no RBD
151 binders were identified for V5) (**Figure 2B and 2E**). A substantial number of the isolated mAbs bound to
152 NTD including 14% for V3, 33% for V5 and 33% for V6 (**Figure 2C and 2E**). These data indicate that RBD
153 and NTD are co-dominant in the context of mRNA-induced plasmablast response. The epitopes for the
154 majority of the remaining spike binding mAbs, 52% for V3, 50% for V5 and 20% for V6, mapped to S2
155 (**Figure 2D and 2E**). Only three mAbs were not accounted for in terms of binding target (two for V3 and
156 one for V5, **Figure 2E**).

157 **The majority of isolated mAbs from SARS-CoV2 vaccinees are non-neutralizing**

158 All antibodies were tested for neutralizing activity against the USA-WA1/2020 strain of SARS-CoV-
159 2. Only a minority of the binding antibodies, even those targeting the RBD, showed neutralizing activity
160 (**Figure 2F and 2G**). For V3, only one (an RBD binder) out of 21 mAbs (5%) displayed neutralizing activity
161 (**Figure 2G**). For V5, a single NTD antibody neutralized authentic SARS-CoV-2 (17%) (**Figure 2G**). The
162 highest frequency of neutralizing antibodies was found in V6 (34%) with one RBD neutralizer and four NTD
163 neutralizers (**Figure 2G**). Interestingly, the highest neutralizing potency was found in mAb PVI.V5-6, an
164 NTD binder followed by PVI.V6-4, an RBD binder.

165 We also tested all the antibodies for reactivity to the spike proteins of the four hCoVs 229E, NL63,
166 HKU1 and OC43. No antibody binding to the spike proteins of α-coronaviruses 229E and NL63 was found
167 but we identified five mAbs (including three from V3, one from V5 and one from V6) that bound, to varying
168 degrees, to the spike of OC43, which, like SARS-CoV-2, is a β-coronavirus (**Figure 2H**). Three mAbs showed
169 strong binding (PVI.V3-8, PVI.V3-12 and PVI.V6-1), while PVI.V3-17 showed an intermediate binding
170 phenotype and PVI-V5-1 bound very weakly. Three of these mAbs also showed binding to the spike of
171 HKU1, another β-coronavirus. Of these, PVI.V6-1 showed only very weak binding while PVI.3-8 and PVI.3-
172 12 had low minimal binding concentrations (MBCs) indicating higher affinity (**Figure 2I**).

173 **The spike-reactive plasmablast response is dominated by IgG1+ cells and is comprised of a mixture of**
174 **cells with low and high levels of somatic hypermutation (SHM)**

175 Single-cell RNA sequencing (scRNAseq) was performed on bulk sorted plasmablasts from the
176 three vaccinees (V3, V5, V6) to comprehensively examine the transcriptional profile, isotype distribution
177 and somatic hypermutation (SHM) of vaccine-induced plasmablasts. We analyzed 4,584, 3,523 and 4,461
178 single cells from subjects V3, V5, and V6, respectively. We first verified the identity of sequenced cells as
179 plasmablasts through the combined expression of B cell receptors (BCRs) (**Figure 3A**) and that of the

180 canonical transcription as well as other factors essential for plasma cell differentiation, such as *PRDM1*,
181 *XBP1* and *MZB1* (**Figure 3B**). To identify vaccine-responding B cell clones among the analyzed
182 plasmablasts, we used scRNAseq to also analyze gene expression and V(D)J libraries from the sorted
183 plasmablasts and clonally matched the BCR sequences to those from which spike-specific mAbs had been
184 made. Using this method, we recovered 332, 7 and 1,384 BCR sequences from the scRNAseq data that are
185 clonally related to the spike-binding mAbs derived from subjects V3, V5 and V6, respectively (**Figure 3C**).
186 It is important to note here that we were not able to recover clonally related sequences for all of the mAbs
187 that we cloned and expressed from each of the three vaccinees.

188 We next examined the isotype and IgG subclass distribution among the recovered sequences.
189 IgG1 was by far the most dominant isotype in the three vaccinees (**Figure 3D**). Finally, we assessed the
190 level of somatic hypermutation (SHM) among the mAbs-related sequences from the three subjects. We
191 used the SHM levels observed in human naïve B cells and seasonal influenza virus vaccination-induced
192 plasmablasts that were previously published for comparison (Turner et al., 2020). Spike-reactive
193 plasmablasts from V3 and V6 but not V5 had accumulated SHM at levels that are significantly greater than
194 those observed with naïve B cells (**Figure 3E, left panel**). Strikingly, the SHM among V6 plasmablasts was
195 equivalent to those observed after seasonal influenza virus vaccination (**Figure 3E, left panel**). We
196 reasoned that the high level of SHM among spike-reactive plasmablasts may be derived from those
197 targeting conserved epitopes that are shared with human β-coronaviruses. Indeed, we found that the
198 SHM level among clones that are related to cross-reactive mAbs was significantly higher than their non-
199 cross-reactive counterparts (**Figure 3E, right panel**).

200 **Competition of RBD binding neutralizing mAbs with ACE2 and affinity of variant RBDs for human ACE2**

201 Two mAbs were identified as neutralizing and binding to RBD. We wanted, therefore, to test if
202 they competed with ACE2 for RBD binding. Concentration-dependent competition was indeed observed
203 for both mAbs demonstrating that inhibition of ACE2 binding is the mechanism of action of the two mAbs
204 (**Figure 4**). Since we prepared RBD proteins of viral variants of concern for analysis of antibody binding
205 (see below), we also wanted to assess the affinity of each variant RBD for human ACE2. Using biolayer
206 interferometry (BLI), we measured association and dissociation rates of the N501Y RBD mutant (B.1.1.7
207 carries that mutation as its sole RBD mutation), Y453F, as found in mink isolates (Larsen et al., 2021),
208 N439K, which is found in some European clades (Thomson et al., 2021), a combination of Y453F and
209 N439K, E484K (part of B.1.351 and P.1) as well as for the B.1.351 and the P.1 RBDs for a recombinant
210 version of human ACE2 (**Figure 4A, 4B and 4D**). Almost all of the single and double mutations in RBD tested
211 increased affinity to human ACE2. Specifically, N501Y and Y453F combined with N439K increased affinity
212 for human ACE2 by 5-fold (**Figure 4D, Suppl. Figure 3**). In contrast, E484K on its own decreased affinity by
213 4-fold. Of note, the B.1.351 RBD affinity for ACE2 was comparable to that of the wild-type RBD. These data
214 were confirmed using an ELISA-based method which showed the same trends (**Suppl. Figure 4**).

215 **Binding profiles of polyclonal serum and mAbs to RBDs carrying mutations found in viral variants of**
216 **concern**

217 Next, we assessed binding of sera from vaccinated individuals, COVID-19 survivors and mAbs
218 derived from plasmablasts to variant RBDs. Our panel of RBDs includes published mAb escape mutants,
219 RBD mutants detected by the Mount Sinai Hospital's Pathogen Surveillance Program in patients seeking
220 care at the Mount Sinai Health System in NYC as well as mutations found in viral variants of interest and
221 variants of concern (Baum et al., 2020; Greaney et al., 2021; Larsen *et al.*, 2021; Thomson *et al.*, 2021;

222 Weisblum *et al.*, 2020). Serum from convalescent individuals showed strong fluctuations depending on
223 the viral variant (**Figure 5A**). In general, single mutants E406Q, E484K and F490K exerted the biggest
224 impact on binding. However, complete loss of binding was rare and 2-4-fold reduction in binding was more
225 common. Interestingly, almost all sera bound better to N501Y RBD (B.1.1.7) than to wild-type RBD
226 (average 129% compared to wild type). Conversely, the B.1.351 RBD caused, on average, a 39% reduction
227 in binding. The impact was slightly lower for the P.1 RBD (average 70% binding compared to wild-type).
228 For sera from the six vaccinated individuals, however, the highest reduction seen was only two-fold for
229 E406Q, N440K, E484K and F490K (**Figure 5B**). Of note, the vaccinees' later samples (V1=d89, V2=d102,
230 V3=d47, V4=d48, V5=49 and V6=48) were assayed to allow for some affinity maturation. The highest
231 reduction observed for E484K, F484A, B.1.351 and P.1 were also approximately two-fold but this did not
232 apply to all six vaccinees. Some vaccinees maintained binding levels against these RBDs at levels
233 comparable to wild-type RBD.

234 RBD binding mAbs were also tested for binding to the same variants. In general, mAbs maintained
235 binding levels within 2-fold of the binding seen with the wild-type RBD with some exceptions. In fact, for
236 most mAbs, no impact on binding was observed (**Figure 5C**) with the exception of PVI.V3-9, which lost
237 binding to the RBD carrying F486A. Although there was a negative impact on binding of several mAbs to
238 the B.1.351 variant, binding was almost unaffected by the mutations in the P.1 variant RBD. Only one
239 mAb, PVI.V6-4, showed a drop in binding to P.1.

240 **Escape of an NTD and E484K mutant virus from polyclonal post-vaccination serum is negligible but**
241 **NTD mutations significantly impact the neutralizing activity of NTD binding mAbs**

242 Through the Mount Sinai Hospital's Pathogen Surveillance Program, we had access to the SARS-
243 CoV-2 isolate PV14252 (Clade 20C, Pango lineage B.1) that featured two mutations (W64R, L141Y) and
244 one deletion (Δ142-145) in the NTD as well as the E484K mutation in the RBD (**Figure 5D**). To determine
245 the susceptibility of this virus variant to neutralization by post-vaccination serum, we performed
246 microneutralization assays. Wild-type SARS-CoV-2 and PV14252 were tested in parallel to ensure that the
247 assay setup for both viruses allowed comparison. We found a relatively minor impact when testing
248 polyclonal sera from vaccinees for neutralizing activity (**Figure 5E**). The activity of sera from V2, V5 and V6
249 slightly increased while the activity for V1, V3 and V4 decreased. Next, we tested the seven neutralizing
250 mAbs that we isolated from plasmablasts. Consistent with their binding profiles in the variant RBD ELISA,
251 the two RBD mAbs neutralized both viruses with comparable efficiency (**Figure 5F**). In fact, the activity of
252 PVI.V3-9 increased slightly (**Figure 5F**). In stark contrast, all five anti-NTD antibodies completely lost
253 neutralizing activity against PV14252 due to mutations present in the NTD of this viral isolate.

254 **B.1.1.7 and B.1.351 partially escape from plasmablast derived neutralizing antibodies**

255 We also tested the neutralizing activity of the two RBD and the five NTD antibodies against the
256 variants of concern B.1.1.7 and B.1.351 (**Figure 5G**). Both variants contain deletions as well as mutations
257 in the NTD. In addition, B.1.1.7 carries the N501Y RBD mutation and B.1.351 carries N417K, E484K and
258 N501Y mutations in the RBD (**Figure 4 A and B**). The two RBD binding antibodies lost no (PVI.V6-4) or little
259 (PVI.V3-9) neutralizing activity against B.1.1.7. However, PVI.V3-9 lost all activity against B.1.351 and the
260 remaining neutralizing activity of PVI.V6-4 was low (but measurable). All but one (PVI.V6-11)) NTD mAbs
261 lost neutralizing activity against B.1.1.7 and all of them lost neutralizing activity against B.1.351 once more
262 highlighting the importance of changes in the NTD on the antibody activity.

263

264 **Discussion**

265 Our knowledge of B-cell responses to SARS-CoV-2 mRNA vaccination remains incomplete. We
266 urgently need information about the nature of polyclonal vaccine-induced responses as well as unbiased,
267 in depth analyses of plasmablast responses. Our data provide important new insights into these responses
268 in comparison with immune responses to natural infection. Indeed, SARS-CoV-2 infection results in a very
269 heterogeneous antibody response to the spike protein in terms of antibody quantity. In contrast, mRNA
270 vaccination appears to induce a high antibody response of relatively homogenous titers. However, we
271 also found that vaccinees generate more non-neutralizing antibodies than COVID-19 survivors resulting in
272 a lower ratio of neutralizing to binding antibodies. These data were already apparent in the early phase
273 clinical trials but remained unrecognized at the time (Walsh et al., 2020). Interestingly, low titer
274 convalescent serum had the highest relative amount of neutralizing antibodies, whereas the proportion
275 of binding antibodies was increased in sera with higher measured antibody titers. The majority of
276 plasmablasts sampled after vaccination do, in fact, produce non-neutralizing antibodies. Two recent
277 studies have performed a similarly unbiased plasmablast analysis for individuals naturally infected with
278 SARS-CoV-2 (Cho et al., 2021; Huang *et al.*, 2021). Of course, the antibody response after SARS-CoV-2
279 infection is not only targeting the spike protein but several other proteins expressed by the virus. When
280 accounting for spike binding only, these studies report proportions of 44% and 25% neutralizing antibodies
281 (Cho *et al.*, 2021; Huang *et al.*, 2021). While plasmablast analysis is in general not quantitative (e.g. one
282 clone per clonotype is selected etc.) our analysis of post-vaccination plasmablasts found a lower number
283 of neutralizing antibodies (17%).

284 Future studies are needed to reveal the role of non-neutralizing antibodies in SARS-CoV-2 immune
285 protection. Indeed, antibody functions other than neutralization have been shown to correlate with
286 protection (Bartsch et al., 2021; Gorman et al., 2021; Schäfer et al., 2021). The importance of absolute
287 antibody titers and not ratios is underscored by the fact that post-vaccination neutralization titers were
288 equal to or exceeded the titers found in the high responder convalescent group.

289 Of the four seasonal CoVs that are widely circulating in humans, β-coronaviruses OC43 and HKU1 have
290 higher homology to SARS-CoV-2 spike. Vaccinated individuals mounted a response to spike proteins from
291 OC43 and HKU1 but not to α-coronaviruses 229E and NL63. This phenomenon resembles the immune
292 imprinting described in influenza virus immunology and has already been shown for natural infection with
293 SARS-CoV-2 where a 'backboost' to β-coronaviruses was also found (Aydillo *et al.*, 2020; Song *et al.*, 2020).
294 A few of the mAbs isolated in our study had, indeed, such a cross-reactive phenotype. It remains unclear
295 whether these antibodies, which target mostly S2 epitopes, contribute to protection against SARS-CoV-2,
296 OC43 or HKU1 infection. However, the cross-reactive epitopes of mAbs that do bind SARS-CoV-2, HKU1
297 and OC43 spikes could provide the basis for future pan-β-coronavirus vaccines. While it is likely the case
298 that the B-cells producing these mAbs come from recall responses and were initially induced by human β-
299 coronaviruses (which is supported by serology and of course the extensive SHM that the mAbs show),
300 they could hypothetically also be *de novo* induced antibodies. While this is probably not the case, we
301 cannot exclude this possibility with our current data.
302

303 Another interesting point we noted is the co-dominance of RBD and NTD. Previous analyses of B-
304 cell responses to SARS-CoV-2 mRNA vaccination focused on cells baited by labeled RBD (Wang *et al.*,
305 2021). We, in contrast, took an unbiased approach to sort and clone plasmablasts in an antigen-agnostic

306 manner. We found similar levels of NTD and RBD binders with many mAbs binding to epitopes outside the
307 RBD and the NTD. In one vaccinee not a single RBD binding mAbs was isolated with the caveats that the
308 overall number of mAbs derived from that individual were low and their polyclonal serum antibody
309 responses included RBD recognition. These data suggest that the NTD, which also harbors neutralizing
310 epitopes, is - at least - as important as the RBD and warrants as much attention. In fact, five out of seven
311 neutralizing antibodies isolated in this study bound to the NTD and only two targeted the RBD. Recent
312 studies analyzing the plasmablast response after natural infection have found a similar co-dominance of
313 RBD and NTD (Cho *et al.*, 2021; Huang *et al.*, 2021) with one study reporting 59 mAbs targeting the RBD,
314 64 targeting the NTD and 46 binding outside of RBD and NTD and the second study finding 10 RBD mAbs,
315 13 non-RBD S1 binding mAbs (strongly suggesting NTD binding) and 9 mAbs targeting S2. Further
316 characterization of the mAbs obtained in our study showed a complete loss of neutralization against an
317 authentic, replication-competent variant virus that harbored extensive changes in the NTD. All NTD mAbs
318 also lost neutralizing activity against B.1.351 and all but one lost activity against B.1.1.7. These
319 observations may explain why a reduction in neutralization against the viral variant of concern B.1.1.7 is
320 seen in some studies despite the fact the N501Y substitution in the RBD of this variant does not
321 significantly impact binding and neutralizing activity (Emary et al., 2021). The key role of NTD as target for
322 antibodies has recently also been shown using memory B cell derived mAbs (McCallum et al., 2021a).

323 In addition, we assessed the impact of different RBD mutations on affinity towards human ACE2.
324 Interestingly, N501Y increased the affinity by five-fold. This increase in receptor binding affinity may
325 contribute to the higher infectivity of B.1.1.7, which carries this mutation in its RBD. In contrast,
326 introduction of E484K reduced the affinity by 4-fold which may explain why virus variants carrying only
327 the E484K mutation have rarely spread efficiently, although viruses carrying E484K have been detected
328 since the fall of 2020 in a handful of patients receiving care at the Mount Sinai Health System and have
329 also been reported in immunocompromised patients (Choi et al., 2020). It is tempting to speculate that
330 the N501Y mutation enables the acquisition of E484K without a fitness loss. In fact, the B.1.351 RBD, which
331 carries N501Y and E484K (as well as N417K) showed binding to hACE2 that was similar to wild- type RBD.
332 Recently, B.1.1.7 variant strains carrying E484K, in addition to N501Y, have been isolated in the UK (PHE,
333 2021), providing evidence for the hypothesis that N501Y enables acquisition of mutations in the RBD that
334 may be detrimental to receptor binding. However, recent expansion of B.1.526, a lineage also featuring
335 E484K but without N501Y in New York City, suggests that this fitness loss may be overcome by other, yet
336 uncharacterized, changes in the virus as well (Annavajhala et al., 2021; Lasek-Nesselquist et al., 2021).
337 Interestingly, binding of convalescent sera to the N501Y RBD was also increased, suggesting that changes
338 that increase affinity for the receptor may also increase affinity of a set of antibodies that may mimic the
339 receptor.

340 We also noted that the two neutralizing antibodies against the RBD showed some reduced binding
341 to a mutant RBD carrying the E484K mutation while having similar or even increased neutralizing potency
342 against a variant virus carrying the E484K mutation as the only change in its RBD. The reduced affinity of
343 the E484K variant RBD for hACE2 could render the virus more susceptible to RBD binding mAbs. Thus, an
344 antibody binding to the RBD may just be more effective in interfering with a low affinity as compared to
345 a high affinity RBD-hACE2 interaction. Increased affinity as an escape mechanism for viruses has been
346 described in the past (Hensley et al., 2009; O'Donnell et al., 2012) and the converse mechanism could be
347 at play here.

Whether or not the current vaccines will provide effective protection against circulating and emerging viral variants of concern is an important question which has gathered a lot of attention in early 2021. Our data indicate that reduction in binding to the E484K and B.1.351 variant RBDs was minor (often only 2-fold) compared to reported reduction in neutralization (which ranges from 6-8 fold to complete loss of neutralization (Cele et al., 2021; Wibmer et al., 2021; Wu et al., 2021)). Although not tested here, it is likely that the reduction in binding to full length spike is even lower, given the many epitopes on the spike other than NTD and RBD. The maintenance of binding to a large degree observed in this study suggests that viral variants will have a minor impact on serological assays which are currently in wide use for medical, scientific and public health reasons. Binding, non-neutralizing antibodies have also been shown to have a protective effect in many viral infections (Asthagiri Arunkumar et al., 2019; Dilillo et al., 2014; Saphire et al., 2018) and may be a factor in the substantial residual protection seen in the Johnson & Johnson and Novavax vaccine trials against B.1.351 in South Africa (Shinde et al., 2021). Production of non-neutralizing antibodies may also play a role in protection by mRNA vaccines after the first dose, as it is substantial and occurs during a time when neutralizing antibody titers are either very low or absent (Baden *et al.*, 2020; Dagan et al., 2021; Polack *et al.*, 2020). Finally, although some antibodies may lose neutralizing activity due to reduced affinity, they do still bind. Furthermore, B cells with these specificities potentially could undergo affinity maturation after exposure to a variant virus or a variant spike-containing vaccine, leading to high affinity antibodies to variant viruses of concern.

In summary, we demonstrate that the antibody responses to SARS-CoV-2 mRNA vaccination comprise a large proportion of non-neutralizing antibodies and are co-dominated by NTD and RBD antibodies. The NTD portion of the spike represents, thus, an important vaccine target. Since all viral variants of concern are heavily mutated in this region, these observations warrant further attention to optimize SARS-CoV-2 vaccines. Finally, broadly cross-reactive mAbs to β-coronavirus spike proteins are induced after vaccination, and suggest a potential development path for a pan- β-coronavirus vaccine.

Acknowledgements

We would like to thank the study participants for their generosity and willingness to participate in longitudinal COVID19 research studies. None of this work would be possible without their contributions. We would like to thank Dr. Randy A. Albrecht for oversight of the conventional BSL3 biocontainment facility, which makes our work with live SARS-CoV-2 possible. We are also grateful for Mount Sinai's leadership during the COVID-19 pandemic. We want to especially thank Drs. Peter Palese, Carlos Cordon-Cardo, Dennis Charney, David Reich and Kenneth Davis for their support. We would also like to thank Bassem Mohamed and Wooseob Kim for their help with preparing the scRNAseq libraries. This work was partially funded by the NIAID Collaborative Influenza Vaccine Innovation Centers (CIVIC) contract 75N93019C00051, NIAID Center of Excellence for Influenza Research and Surveillance (CEIRS, contract # HHSN272201400008C and HHSN272201400006C), NIAID grants U01AI141990 and U01AI150747, by the generous support of the JPB Foundation and the Open Philanthropy Project (research grant 2020-215611 (5384); and by anonymous donors. J.S.T. was supported by NIAID 5T32CA009547.

Conflict of interest statement

389 The Icahn School of Medicine at Mount Sinai has filed patent applications relating to SARS-CoV-2
390 serological assays and NDV-based SARS-CoV-2 vaccines which list Florian Krammer as co-inventor. Viviana
391 Simon is also listed on the serological assay patent application as co-inventors. Mount Sinai has spun out
392 a company, Kantaro, to market serological tests for SARS-CoV-2. Florian Krammer has consulted for Merck
393 and Pfizer (before 2020), and is currently consulting for Pfizer, Seqirus and Avimex. The Krammer
394 laboratory is also collaborating with Pfizer on animal models of SARS-CoV-2. Ali Ellebedy has consulted for
395 InBios and Fimbrion Therapeutics (before 2021) and is currently a consultant for Mubadala Investment
396 Company. The Ellebedy laboratory received funding under sponsored research agreements that are
397 unrelated to the data presented in the current study from Emergent BioSolutions and from AbbVie.
398

399 **Materials and methods.**

400 **Human subjects and specimen collection**. The study protocols for the collection of clinical specimens from
401 individuals with and without SARS-CoV-2 infection by the Personalized Virology Initiative were reviewed
402 and approved by the Mount Sinai Hospital Institutional Review Board (IRB-16-16772; IRB-16-00791; IRB-
403 20-03374). All participants provided written informed consent prior to collection of specimen and clinical
404 information. All specimens were coded prior to processing and analysis. An overview of the characteristics
405 of the vaccinees as well as the study participants with and without COVID-19 is provided in **Suppl. Table**
406 **1**. The vaccinees received two doses of the Pfizer mRNA vaccine.

407 Whole blood was collected via phlebotomy in serum separator tubes (SST) or ethylenediaminetetraacetic
408 acid (EDTA) tubes. Serum was collected after centrifucation as per manufacturers' instructions. Peripheral
409 blood mononuclear cells (PBMCs) isolation was performed by density gradient centrifugation using
410 SepMate tubes (Stemcell) according to manufacturers' instructions. PBMCs were cryo-preserved and
411 stored in liquid nitrogen until analysis.

412 **Recombinant proteins.** All recombinant proteins were produced using Expi293F cells (Life Technologies).
413 Receptor binding domain (RBD) and spike protein of SARS-CoV-2 (GenBank: MN908947.3) was cloned into
414 a mammalian expression vector, pCAGGS as described earlier (Amanat et al., 2020b; Stadlbauer et al.,
415 2020). RBD mutants were generated in the pCAGGS RBD construct by changing single residues using
416 mutagenesis primers. All proteins were purified after transient transfections with each respective plasmid.
417 Six-hundred million Expi293F cells were transfected using the ExpiFectamine 293 Transfection Kit and
418 purified DNA. Supernatants were collected on day four post transfection, centrifuged at 4,000 g for 20
419 minutes and finally, the supernatant was filtered using a 0.22 um filter. Ni-NTA agarose (Qiagen) was used
420 to purify the protein via gravity flow and proteins were eluted as previously described (Amanat *et al.*,
421 2020b; Stadlbauer *et al.*, 2020). The buffer was exchanged using Amicon centrifugal units (EMD Millipore)
422 and all recombinant proteins were finally re-suspended in phosphate buffered saline (PBS). Proteins were
423 also run on a sodium dodecyl sulphate (SDS) polyacrylamide gels (5–20% gradient; Bio-Rad) to check for
424 purity (Amanat et al., 2018; Margine et al., 2013). Plasmids to express recombinant spike proteins of 229E,
425 HKU1, NL63 and OC43 were generously provided by Dr. Barney Graham (Pallesen et al., 2017). NTD and
426 S2 proteins were purchased from SinoBiologics.

427

428 **ELISA**. Ninety-six well plates (Immulon 4 HBX; Thermo Scientific) were coated overnight at 4°C with
429 recombinant proteins at a concentration of 2 ug/ml in PBS (Gibco; Life Technologies) and 50 uls/well. The
430 next day, the coating solution was discarded. One hundred uls per well of 3% non-fat milk prepared in PBS

431 (Life Technologies) containing 0.01% Tween-20 (TPBS; Fisher Scientific) was added to the plates to block
432 the plates for 1 hour at room temperature (RT). All serum dilutions were prepared in 1% non-fat milk
433 prepared in TPBS. All serum samples were diluted 3-fold starting at a dilution of 1:50. After the blocking
434 step, serum dilutions were added to the respective plates for two hours at RT. Next, plates were washed
435 thrice with 250 uls/well of TPBS to remove any residual primary antibody. Secondary antibody solution
436 was prepared in 1% non-fat milk in TPBS as well and 100 uls/well was added to the plates for 1 hour at
437 RT. For human samples, anti-human IgG conjugated to horseradish peroxidase (HRP) was used at a
438 dilution of 1:3000 (Millipore Sigma; catalog #A0293). For mouse samples, anti-mouse IgG conjugated to
439 HRP was used at the same dilution (Rockland antibodies and assays; catalog #610-4302). Specifically, a
440 mouse anti-histidine antibody (Takara; catalog #631212) was used as a positive control to detect proteins
441 with a hexa-histidine tag. Once the secondary incubation was done, plates were again washed thrice with
442 250uls/well of TPBS. Developing solution was made in 0.05M phosphate-citrate buffer at pH 5 using o-
443 phenylenediamine dihydrochloride tablets (Sigma-Aldrich; OPD) at a final concentration of 0.04 mg/ml.
444 One hundred uls/well of developing solution was added to each plate for exactly 10 minutes after which
445 the reaction was halted with addition of 50 uls/well of 3M hydrochloric acid (HCl). Plates were read at an
446 optical density of 490 nanometers using a Synergy 4 (BioTek) plate reader. Eight wells on each plate
447 received no primary antibody (blank wells) and the optical density in those wells was used to assess
448 background. Area under the curve was calculated by deducting the average of blank values plus 3 times
449 standard deviation of the blank values. All data was analyzed in Graphpad Prism 7. This protocol has been
450 described in detail earlier (Bailey et al., 2019; Wohlbold et al., 2015).

451 Purified monoclonal antibodies were used at a concentration of 30 ug/ml and then subsequently diluted
452 3-fold. Purified monoclonal antibodies were only incubated on the coated plates for an hour. The
453 remaining part of the protocol was the same as above (Amanat et al., 2020a; Wohlbold et al., 2016).

454 **Bio-layer Interferometry Binding Experiments**. Bio-layer Interferometry (BLI) experiments were
455 performed using the BLItz system (fortéBIO, Pall Corporation). Recombinant human Fc fusion ACE2
456 (SinoBiological) was immobilized on an anti-human IgG Fc biosensor, and RBDs were then applied to
457 obtain binding affinities. Single-hit concentrations were tested at 5.8 µM for binding. All measurements
458 were repeated in subsequent independent experiments. K_D values were obtained through local fit of the
459 curves by applying a 1:1 binding isotherm model using vendor-supplied software. All experiments were
460 performed in PBS pH 7.4 and at room temperature.
461
462 **hACE2 competition interferometry experiments,** Interferometry experiments were performed using a
463 BLItz instrument (fortéBIO, Sartorius). Polyhistidine-tagged Fabs were immobilized on Ni-NTA biosensors
464 at 10 µg/ml and SARS-CoV-2 RBD was supplied as analyte at 5µM alone or pre-mixed with hACE2-Fc at
465 different concentrations. Maximal signal at association (Rmax) was used to plot the concentration-
466 dependent competition with hACE2. All experiments were performed in PBS at pH 7.4 and at room
467 temperature.
468
469 **RBD-hACE2 ELISA.** 25ng of hACE2-Fc fusion protein expressed in HEK293 cells were adhered to high-
470 capacity binding, 96 well-plates (Corning) overnight in PBS. Plates were blocked with 5% BSA in PBS
471 containing Tween-20 (PBS-T) for 1hr at room temperature (RT). Blocking solution was discarded and 5-
472 fold dilutions of 6xHis-tagged RBDs in PBS were added to wells and incubated for 1hr at RT. Plates were
473 then washed three times with PBS-T. Anti-polyhistidine IgG-Biotin (Abcam) in PBS-T was added to each
474 and incubated for 1hr at RT. Plates were then washed three times with PBS-T. Streptavidin-HRP (Abcam)
475 in PBS-T was added to each and incubated for 1hr at RT. Plates were then washed three times with PBS-T

476 Plates were developed using 1-Step Ultra TMB substrate (ThermoFisher), stopped with sulfuric acid and
477 immediately read using a plate reader at 450nm. Data were plotted using Prism 9 (GraphPad Software)
478 and affinities determined by applying a nonlinear regression model.
479
480 **Viruses and cells.** Vero.E6 cells (ATCC #CRL-1586) cells were maintained in culture using Dulbecco's
481 Modified Eagles Medium (DMEM, Gibco) which was supplemented with 10% fetal bovine serum (FBS,
482 Corning) and antibiotics solution containing 10,000 units/mL of penicillin and 10,000 µg/mL of
483 streptomycin (Pen Strep, Gibco)(10). Wild type SARS-CoV-2 (isolate USA-WA1/2020), hCoV-19/South
484 Africa/KRISP-K005325/2020 (B.1.351, BEI Resources NR-54009) and hCoV-19/England/204820464/2020
485 (B.1.1.7, BEI Resources NR-54000) were grown in cells for 3 days, the supernatant was clarified by
486 centrifugation at 4,000 g for 5 minutes and aliquots were frozen at -80°C for long term use. The viruses
487 were subjected to deep sequencing to ensure that no mutations had taken place in culture. The polybasic
488 cleavage site changed to WRAR in the B.1.351 variant virus during cultivation in cell culture (as known for
489 this virus at BEI Resources) and no other unexpected mutations occurred. A primary virus isolate,
490 PV14252, bearing mutations and deletions in the spike was obtained by incubating 200 uls of viral
491 transport media from the nasopharyngeal swab with Vero.E6 cells. The sequence of the passage 2 viral
492 isolate was identical to the sequence obtained directly from the clinical specimen. Sequencing was
493 performed on the Illumina platform as described previously (Gonzalez-Reiche et al., 2020). Both
494 replication competent viruses were used to test serum from study participants and antibodies for
495 neutralization activity.
496
497 **Neutralization assay.** Twenty-thousand cells in 100 uls per well were seeded on sterile 96-well cell culture
498 plates one day prior to the neutralization assay. In general, cells were used at 90% confluency to perform
499 the assay. All serum samples were heat-inactivated to eliminate any complement activity. Serial dilutions
500 of serum samples were made in 1X minimal essential medium (MEM; Life Technologies) starting at a
501 dilution of 1:20. All work with authentic SARS-CoV-2 (isolate USA-WA1/2020 and PV14252) was done in a
502 biosafety level 3 (BSL3) laboratory following institutional biosafety guidelines and has been described in
503 much greater detail earlier (Amanat *et al.*, 2020b; Amanat et al., 2020c). Six hundred median cell culture
504 infectious doses ($TCID_{50}$s) of authentic virus (USA-WA1/2020 and PV14252) was added to each serum
505 dilution and virus-serum mixture was incubated together for 1 hour inside the biosafety cabinet. Media
506 from the cells was removed and 120 uls of the virus-serum mixture was added onto the cells for 1 hour at
507 37°C. After one hour, the virus-serum mixture was removed and 100 uls of each corresponding dilution
508 was added to every well. In addition, 100uls of 1X MEM was also added to every well. Cells were incubated
509 for 48 hours at 37°C after which the media was removed and 150 uls of 10% formaldehyde (Polysciences)
510 was added to inactivate the virus. For assay control, remdesivir was used against both the wild type virus
511 as well as the patient isolate. After 24 hours, cells were permeabilized and stained using an anti-
512 nucleoprotein antibody 1C7 as discussed in detail earlier (Amanat *et al.*, 2020b; Sun et al., 2020).

513 **Cell sorting and flow cytometry.** Staining for sorting was performed using cryo-preserved PBMCs in 2%
514 FBS and 2 mM ethylenediaminetetraacetic acid (EDTA) in PBS (P2). Cells were stained for 30 min on ice
515 with CD20-Pacific Blue (2H7, 1:400), Zombie Aqua, CD71-FITC (CY1G4, 1:200), IgD-PerCP-Cy5.5 (IA6-2,
516 1:200), CD19-PE (HIB19, 1:200), CD38-PE-Cy7 (HIT2, 1:200), and CD3-Alexa 700 (HIT3a, 1:200), all
517 BioLegend. Cells were washed twice, and single plasmablasts (live singlet $CD19^{+}$ $CD3^{-}$ IgD^{lo} $CD38^{+}$ $CD20^{-}$
518 $CD71^{+}$) were sorted using a FACSAria II into 96-well plates containing 2 µL Lysis Buffer (Clontech)
519 supplemented with 1 U/µL RNase inhibitor (NEB) and immediately frozen on dry ice, or bulk sorted into
520 PBS supplemented with 0.05% BSA and processed for single cell RNAseq.

521 **Monoclonal antibody (mAb) generation.** Antibodies were cloned as described previously (Wrammert et
522 al., 2011). Briefly, VH, Vκ, and Vλ genes were amplified by reverse transcription-PCR and nested PCR

523 reactions from singly sorted plasmablasts using primer combinations specific for IgG, IgM/A, Igκ, and Igλ
524 from previously described primer sets (Smith et al., 2009) and then sequenced. To generate recombinant
525 antibodies, restriction sites were incorporated via PCR with primers to the corresponding heavy and light
526 chain V and J genes. The amplified VH, Vκ, and Vλ genes were cloned into IgG1 and Igκ expression vectors,
527 respectively, as described previously (Nachbagauer et al., 2018; Wrammert et al., 2008). Heavy and light
528 chain plasmids were co-transfected into Expi293F cells (Gibco) for expression, and antibody was purified
529 with protein A agarose (Invitrogen).

530 **Single-cell RNAseq library preparation and sequencing.** Bulk-sorted plasmablasts were processed using
531 the following 10× Genomics kits: Chromium Next GEM Single Cell 5' Kit v2 (PN-1000263); Library
532 Construction Kit (PN-1000190); Chromium Next GEM Chip K Single Cell Kit (PN-1000286); Chromium Single
533 Cell Human BCR Amplification Kit (PN- 1000253), and Dual Index Kit TT Set A (PN-1000215). The cDNAs
534 were prepared after GEM generation and barcoding, followed by GEM RT reaction and bead cleanup
535 steps. Purified cDNA was amplified for 10–14 cycles before cleaning with SPRIselect beads. Then, samples
536 were evaluated on a 4200 TapeStation (Agilent) to determine cDNA concentration. B-cell receptor (BCR)
537 target enrichments were performed on full-length cDNA. Gene expression and enriched BCR libraries were
538 prepared as recommended by the Chromium Next GEM Single Cell 5' Reagent Kits v2 (Dual Index) user
539 guide, with appropriate modifications to the PCR cycles based on the calculated cDNA concentration. The
540 cDNA libraries were sequenced on Novaseq S4 (Illumina), targeting a median sequencing depth of 50,000
541 and 5,000 read pairs per cell for gene expression and BCR libraries, respectively.

542 **Single cell RNAseq analysis.** Single-cell RNA sequencing and BCR sequencing data was processed using
543 Cell Ranger v5.0 and the GRCh38-2020 version of the human genome provided by the manufacturer. Total
544 recovered cells by RNA sequencing were V3: 6,608, V5: 5,256, and V6: 6,325 with a mean of 90.64% read
545 mapped to the genome. Count matrices were processed in R (v4.0.2) using the Seurat (v3.2.2) R package
546 (Stuart et al., 2019). Cells were filtered for percentage of mitochondrial genes less than 15% and number
547 features less than 4,000. The three specimen sequencing runs were integrated using log-normalized count
548 values and canonical correlation approach (Stuart *et al.*, 2019) with 2,000 variable features. The resulting
549 single-cell object underwent principal component analysis and the top 30 principal components were used
550 for uniform manifold approximation and projection and identifying neighbors. Clustering was performed
551 using a resolution of 0.6. The integrated RNA sequencing object included 12,568 cells with V3: 4,584, V5:
552 3,523, and V6: 4,461 cells. The filtered contig annotation output of Cell Ranger vdj were loaded into R and
553 processed using the scRepertoire (v1.1.3) R package (Borcherding et al., 2020). Clonotypes were assigned
554 using igraph (v1.2.6) network analysis of components generated from CDR3 sequences greater than or
555 equal to 0.85 normalized Levenshtein distance. Percent of cells expressing genes along the UMAP
556 embedding was visualized using the schex (v1.3.0) R package. For mutation analysis, heavy chains of mAbs
557 and single-cell BCRs first underwent V(D)J gene annotation using IgBLAST (v1.14.0) (Ye et al., 2013) with
558 human reference (release 201931-4) from the international ImMunoGeneTics information system (IMGT)
559 (Giudicelli et al., 2005) and then parsing using Change-O (v0.4.6) (Gupta et al., 2015). Mutation frequency
560 was calculated, as described in (Turner *et al.*, 2020), using the "calcObservedMutations" function from
561 SHazaM (v.1.0.2) (Gupta *et al.*, 2015) and by counting the number of nucleotide mismatches from the
562 germline sequence in the heavy chain variable segment leading up to the complementary-determining
563 region 3 (CDR3), while excluding the first 18 positions that could be error-prone due to the primers used
564 for generating the mAb sequences.

565

566 **Structure visualization and statistical analysis.** Structural figures were modeled and rendered in Pymol
567 (The PyMOL Molecular Graphics System, Version 2.4 Schrödinger, LLC). Statistical analysis was performed
568 in GraphPad Prism using a one-way ANOVA with correction for multiple comparisons.

569

570 **References**

571 Amanat, F., Duehr, J., Huang, C., Paessler, S., Tan, G.S., and Krammer, F. (2020a). Monoclonal Antibodies
572 with Neutralizing Activity and Fc-Effector Functions against the Machupo Virus Glycoprotein. J Virol *94*.
573 10.1128/JVI.01741-19.
574 Amanat, F., Duehr, J., Oestereich, L., Hastie, K.M., Ollmann Saphire, E., and Krammer, F. (2018).
575 Antibodies to the Glycoprotein GP2 Subunit Cross-React between Old and New World Arenaviruses.
576 mSphere *3*. 10.1128/mSphere.00189-18.
577 Amanat, F., Stadlbauer, D., Strohmeier, S., Nguyen, T.H.O., Chromikova, V., McMahon, M., Jiang, K.,
578 Arunkumar, G.A., Jurczyszak, D., Polanco, J., et al. (2020b). A serological assay to detect SARS-CoV-2
579 seroconversion in humans. Nat Med *26*, 1033-1036. 10.1038/s41591-020-0913-5.
580 Amanat, F., White, K.M., Miorin, L., Strohmeier, S., McMahon, M., Meade, P., Liu, W.C., Albrecht, R.A.,
581 Simon, V., Martinez-Sobrido, L., et al. (2020c). An In Vitro Microneutralization Assay for SARS-CoV-2
582 Serology and Drug Screening. Curr Protoc Microbiol *58*, e108. 10.1002/cpmc.108.
583 Annavajhala, M.K., Mohri, H., Zucker, J.E., Sheng, Z., Wang, P., Gomez-Simmonds, A., Ho, D.D., and
584 Uhlemann, A.C. (2021). A Novel SARS-CoV-2 Variant of Concern, B.1.526, Identified in New York.
585 medRxiv. 10.1101/2021.02.23.21252259.
586 Asthagiri Arunkumar, G., Ioannou, A., Wohlbold, T.J., Meade, P., Aslam, S., Amanat, F., Ayllon, J., García-
587 Sastre, A., and Krammer, F. (2019). Broadly Cross-Reactive, Nonneutralizing Antibodies against Influenza
588 B Virus Hemagglutinin Demonstrate Effector Function-Dependent Protection against Lethal Viral
589 Challenge in Mice. J Virol *93*. 10.1128/JVI.01696-18.
590 Aydillo, T., Rombauts, A., Stadlbauer, D., Aslam, S., Abelenda-Alonso, G., Escalera, A., Amanat, F., Jiang,
591 K., Krammer, F., Carratala, J., and García-Sastre, A. (2020). Antibody Immunological Imprinting on
592 COVID-19 Patients. medRxiv, 2020.2010.2014.20212662. 10.1101/2020.10.14.20212662.
593 Baden, L.R., El Sahly, H.M., Essink, B., Kotloff, K., Frey, S., Novak, R., Diemert, D., Spector, S.A., Rouphael,
594 N., Creech, C.B., et al. (2020). Efficacy and Safety of the mRNA-1273 SARS-CoV-2 Vaccine. N Engl J Med.
595 10.1056/NEJMoa2035389.
596 Bailey, M.J., Broecker, F., Duehr, J., Arumemi, F., Krammer, F., Palese, P., and Tan, G.S. (2019).
597 Antibodies Elicited by an NS1-Based Vaccine Protect Mice against Zika Virus. mBio *10*.
598 10.1128/mBio.02861-18.
599 Barnes, C.O., West, A.P., Huey-Tubman, K.E., Hoffmann, M.A.G., Sharaf, N.G., Hoffman, P.R., Koranda,
600 N., Gristick, H.B., Gaebler, C., Muecksch, F., et al. (2020). Structures of Human Antibodies Bound to
601 SARS-CoV-2 Spike Reveal Common Epitopes and Recurrent Features of Antibodies. Cell *182*, 828-
602 842.e816. 10.1016/j.cell.2020.06.025.
603 Bartsch, Y.C., Fischinger, S., Siddiqui, S.M., Chen, Z., Yu, J., Gebre, M., Atyeo, C., Gorman, M.J., Zhu, A.L.,
604 Kang, J., et al. (2021). Discrete SARS-CoV-2 antibody titers track with functional humoral stability. Nat
605 Commun *12*, 1018. 10.1038/s41467-021-21336-8.
606 Baum, A., Fulton, B.O., Wloga, E., Copin, R., Pascal, K.E., Russo, V., Giordano, S., Lanza, K., Negron, N., Ni,
607 M., et al. (2020). Antibody cocktail to SARS-CoV-2 spike protein prevents rapid mutational escape seen
608 with individual antibodies. Science *369*, 1014-1018. 10.1126/science.abd0831.
609 Borcherding, N., Bormann, N.L., and Kraus, G. (2020). scRepertoire: An R-based toolkit for single-cell
610 immune receptor analysis. F1000Res *9*, 47. 10.12688/f1000research.22139.2.

611 Cao, Y., Su, B., Guo, X., Sun, W., Deng, Y., Bao, L., Zhu, Q., Zhang, X., Zheng, Y., Geng, C., et al. (2020).
612 Potent Neutralizing Antibodies against SARS-CoV-2 Identified by High-Throughput Single-Cell Sequencing
613 of Convalescent Patients' B Cells. Cell *182*, 73-84.e16. 10.1016/j.cell.2020.05.025.
614 Carvalho, T., Krammer, F., and Iwasaki, A. (2021). The first 12 months of COVID-19: a timeline of
615 immunological insights. Nat Rev Immunol *21*, 245-256. 10.1038/s41577-021-00522-1.
616 Cele, S., Gazy, I., Jackson, L., Hwa, S.-H., Tegally, H., Lustig, G., Giandhari, J., Pillay, S., Wilkinson, E.,
617 Naidoo, Y., et al. (2021). Escape of SARS-CoV-2 501Y.V2 variants from neutralization by convalescent
618 plasma. medRxiv, 2021.2001.2026.21250224. 10.1101/2021.01.26.21250224.
619 Chi, X., Yan, R., Zhang, J., Zhang, G., Zhang, Y., Hao, M., Zhang, Z., Fan, P., Dong, Y., Yang, Y., et al. (2020).
620 A neutralizing human antibody binds to the N-terminal domain of the Spike protein of SARS-CoV-2.
621 Science *369*, 650-655. 10.1126/science.abc6952.
622 Cho, H., Gonzales-Wartz, K.K., Huang, D., Yuan, M., Peterson, M., Liang, J., Beutler, N., Torres, J.L., Cong,
623 Y., Postnikova, E., et al. (2021). Ultrapotent bispecific antibodies neutralize emerging SARS-CoV-2
624 variants. bioRxiv, 2021.2004.2001.437942. 10.1101/2021.04.01.437942.
625 Choi, B., Choudhary, M.C., Regan, J., Sparks, J.A., Padera, R.F., Qiu, X., Solomon, I.H., Kuo, H.H., Boucau,
626 J., Bowman, K., et al. (2020). Persistence and Evolution of SARS-CoV-2 in an Immunocompromised Host.
627 N Engl J Med *383*, 2291-2293. 10.1056/NEJMc2031364.
628 Dagan, N., Barda, N., Kepten, E., Miron, O., Perchik, S., Katz, M.A., Hernán, M.A., Lipsitch, M., Reis, B.,
629 and Balicer, R.D. (2021). BNT162b2 mRNA Covid-19 Vaccine in a Nationwide Mass Vaccination Setting. N
630 Engl J Med. 10.1056/NEJMoa2101765.
631 Dan, J.M., Mateus, J., Kato, Y., Hastie, K.M., Yu, E.D., Faliti, C.E., Grifoni, A., Ramirez, S.I., Haupt, S.,
632 Frazier, A., et al. (2021). Immunological memory to SARS-CoV-2 assessed for up to 8 months after
633 infection. Science *371*. 10.1126/science.abf4063.
634 Davies, N.G., Abbott, S., Barnard, R.C., Jarvis, C.I., Kucharski, A.J., Munday, J.D., Pearson, C.A.B., Russell,
635 T.W., Tully, D.C., Washburne, A.D., et al. (2021). Estimated transmissibility and impact of SARS-CoV-2
636 lineage B.1.1.7 in England. Science, eabg3055. 10.1126/science.abg3055.
637 Dilillo, D.J., Tan, G.S., Palese, P., and Ravetch, J.V. (2014). Broadly neutralizing hemagglutinin stalk-
638 specific antibodies require FcγR interactions for protection against influenza virus in vivo. Nat Med.
639 10.1038/nm.3443.
640 Emary, K.R.W., Golubchik, T., Aley, P.K., Ariani, C.V., Angus, B., Bibi, S., Blane, B., Bonsall, D., Cicconi, P.,
641 Charlton, S., et al. (2021). Efficacy of ChAdOx1 nCoV-19 (AZD1222) vaccine against SARS-CoV-2 variant of
642 concern 202012/01 (B.1.1.7): an exploratory analysis of a randomised controlled trial. Lancet *397*, 1351-
643 1362. 10.1016/S0140-6736(21)00628-0.
644 Faria, N.R., Claro, I.M., Candido, D., Franco, L.A.M., Andrade, P.S., Coletti, T.M., Silva, C.A.M., Sales, F.C.,
645 Manula, E.R., Aguiar, R.S., et al. (2021). <h1 data-topic-id="586" style="font-size: 1.7511em; margin: 0px
646 0px 4px; font-family: Helvetica, Arial, sans-serif; width: 999px; line-height: 1.2; overflow-wrap: break-
647 word; color: rgb(34, 34, 34); background-color: rgb(255, 255, 255);">Genomic characterisation of an
648 emergent SARS-CoV-2 lineage in Manaus: preliminary findings.
649 Gaebler, C., Wang, Z., Lorenzi, J.C.C., Muecksch, F., Finkin, S., Tokuyama, M., Ladinsky, M., Cho, A.,
650 Jankovic, M., Schaefer-Babajew, D., et al. (2020). Evolution of Antibody Immunity to SARS-CoV-2.
651 bioRxiv. 10.1101/2020.11.03.367391.
652 Giudicelli, V., Chaume, D., and Lefranc, M.P. (2005). IMGT/GENE-DB: a comprehensive database for
653 human and mouse immunoglobulin and T cell receptor genes. Nucleic Acids Res *33*, D256-261.
654 10.1093/nar/gki010.
655 Gonzalez-Reiche, A.S., Hernandez, M.M., Sullivan, M.J., Ciferri, B., Alshammary, H., Obla, A., Fabre, S.,
656 Kleiner, G., Polanco, J., Khan, Z., et al. (2020). Introductions and early spread of SARS-CoV-2 in the New
657 York City area. Science. 10.1126/science.abc1917.

658 Gorman, M.J., Patel, N., Guebre-Xabier, M., Zhu, A., Atyeo, C., Pullen, K.M., Loos, C., Goez-Gazi, Y.,
659 Carrion, R., Tian, J.-H., et al. (2021). Collaboration between the Fab and Fc contribute to maximal
660 protection against SARS-CoV-2 in nonhuman primates following NVX-CoV2373 subunit vaccine with
661 Matrix-M™ vaccination. bioRxiv, 2021.2002.2005.429759. 10.1101/2021.02.05.429759.
662 Grandjean, L., Saso, A., Torres, A., Lam, T., Hatcher, J., Thistlethwayte, R., Harris, M., Best, T., Johnson,
663 M., Wagstaffe, H., et al. (2020). Humoral Response Dynamics Following Infection with SARS-CoV-2.
664 medRxiv, 2020.2007.2016.20155663. 10.1101/2020.07.16.20155663.
665 Greaney, A.J., Starr, T.N., Gilchuk, P., Zost, S.J., Binshtein, E., Loes, A.N., Hilton, S.K., Huddleston, J.,
666 Eguia, R., Crawford, K.H.D., et al. (2021). Complete Mapping of Mutations to the SARS-CoV-2 Spike
667 Receptor-Binding Domain that Escape Antibody Recognition. Cell Host Microbe *29*, 44-57.e49.
668 10.1016/j.chom.2020.11.007.
669 Gupta, N.T., Vander Heiden, J.A., Uduman, M., Gadala-Maria, D., Yaari, G., and Kleinstein, S.H. (2015).
670 Change-O: a toolkit for analyzing large-scale B cell immunoglobulin repertoire sequencing data.
671 Bioinformatics *31*, 3356-3358. 10.1093/bioinformatics/btv359.
672 Guthmiller, J.J., Stovicek, O., Wang, J., Changrob, S., Li, L., Halfmann, P., Zheng, N.Y., Utset, H., Stamper,
673 C.T., Dugan, H.L., et al. (2021). SARS-CoV-2 Infection Severity Is Linked to Superior Humoral Immunity
674 against the Spike. mBio *12*. 10.1128/mBio.02940-20.
675 Hensley, S.E., Das, S.R., Bailey, A.L., Schmidt, L.M., Hickman, H.D., Jayaraman, A., Viswanathan, K.,
676 Raman, R., Sasisekharan, R., Bennink, J.R., and Yewdell, J.W. (2009). Hemagglutinin receptor binding
677 avidity drives influenza A virus antigenic drift. Science *326*, 734-736. 10.1126/science.1178258.
678 Huang, K.A., Tan, T.K., Chen, T.H., Huang, C.G., Harvey, R., Hussain, S., Chen, C.P., Harding, A., Gilbert-
679 Jaramillo, J., Liu, X., et al. (2021). Breadth and function of antibody response to acute SARS-CoV-2
680 infection in humans. PLoS Pathog *17*, e1009352. 10.1371/journal.ppat.1009352.
681 Isho, B., Abe, K.T., Zuo, M., Jamal, A.J., Rathod, B., Wang, J.H., Li, Z., Chao, G., Rojas, O.L., Bang, Y.M., et
682 al. (2020). Persistence of serum and saliva antibody responses to SARS-CoV-2 spike antigens in COVID-19
683 patients. Sci Immunol *5*. 10.1126/sciimmunol.abe5511.
684 Iyer, A.S., Jones, F.K., Nodoushani, A., Kelly, M., Becker, M., Slater, D., Mills, R., Teng, E., Kamruzzaman,
685 M., Garcia-Beltran, W.F., et al. (2020). Dynamics and significance of the antibody response to SARS-CoV-
686 2 infection. medRxiv. 10.1101/2020.07.18.20155374.
687 Krammer, F. (2020). SARS-CoV-2 vaccines in development. Nature *586*, 516-527. 10.1038/s41586-020-
688 2798-3.
689 Lan, J., Ge, J., Yu, J., Shan, S., Zhou, H., Fan, S., Zhang, Q., Shi, X., Wang, Q., Zhang, L., and Wang, X.
690 (2020). Structure of the SARS-CoV-2 spike receptor-binding domain bound to the ACE2 receptor. Nature
691 *581*, 215-220. 10.1038/s41586-020-2180-5.
692 Larsen, H.D., Fonager, J., Lomholt, F.K., Dalby, T., Benedetti, G., Kristensen, B., Urth, T.R., Rasmussen, M.,
693 Lassaunière, R., Rasmussen, T.B., et al. (2021). Preliminary report of an outbreak of SARS-CoV-2 in mink
694 and mink farmers associated with community spread, Denmark, June to November 2020. Euro Surveill
695 *26*. 10.2807/1560-7917.ES.2021.26.5.210009.
696 Lasek-Nesselquist, E., Lapierre, P., Schneider, E., George, K.S., and Pata, J. (2021). The localized rise of a
697 B.1.526 SARS-CoV-2 variant containing an E484K mutation in New York State. medRxiv,
698 2021.2002.2026.21251868. 10.1101/2021.02.26.21251868.
699 Letko, M., Marzi, A., and Munster, V. (2020). Functional assessment of cell entry and receptor usage for
700 SARS-CoV-2 and other lineage B betacoronaviruses. Nat Microbiol *5*, 562-569. 10.1038/s41564-020-
701 0688-y.
702 Liu, L., Wang, P., Nair, M.S., Yu, J., Rapp, M., Wang, Q., Luo, Y., Chan, J.F., Sahi, V., Figueroa, A., et al.
703 (2020). Potent neutralizing antibodies against multiple epitopes on SARS-CoV-2 spike. Nature *584*, 450-
704 456. 10.1038/s41586-020-2571-7.

705 Margine, I., Palese, P., and Krammer, F. (2013). Expression of functional recombinant hemagglutinin and
706 neuraminidase proteins from the novel H7N9 influenza virus using the baculovirus expression system. J
707 Vis Exp, e51112. 10.3791/51112.
708 McCallum, M., De Marco, A., Lempp, F.A., Tortorici, M.A., Pinto, D., Walls, A.C., Beltramello, M., Chen,
709 A., Liu, Z., Zatta, F., et al. (2021a). N-terminal domain antigenic mapping reveals a site of vulnerability for
710 SARS-CoV-2. Cell. 10.1016/j.cell.2021.03.028.
711 McCallum, M., Marco, A., Lempp, F., Tortorici, M.A., Pinto, D., Walls, A.C., Beltramello, M., Chen, A., Liu,
712 Z., Zatta, F., et al. (2021b). N-terminal domain antigenic mapping reveals a site of vulnerability for SARS-
713 CoV-2. bioRxiv. 10.1101/2021.01.14.426475.
714 Nachbagauer, R., Shore, D., Yang, H., Johnson, S.K., Gabbard, J.D., Tompkins, S.M., Wrammert, J.,
715 Wilson, P.C., Stevens, J., Ahmed, R., et al. (2018). Broadly Reactive Human Monoclonal Antibodies
716 Elicited following Pandemic H1N1 Influenza Virus Exposure Protect Mice against Highly Pathogenic H5N1
717 Challenge. J Virol *92*. 10.1128/JVI.00949-18.
718 O'Donnell, C.D., Vogel, L., Wright, A., Das, S.R., Wrammert, J., Li, G.M., McCausland, M., Zheng, N.Y.,
719 Yewdell, J.W., Ahmed, R., et al. (2012). Antibody pressure by a human monoclonal antibody targeting
720 the 2009 pandemic H1N1 virus hemagglutinin drives the emergence of a virus with increased virulence
721 in mice. mBio *3*. 10.1128/mBio.00120-12.
722 Pallesen, J., Wang, N., Corbett, K.S., Wrapp, D., Kirchdoerfer, R.N., Turner, H.L., Cottrell, C.A., Becker,
723 M.M., Wang, L., Shi, W., et al. (2017). Immunogenicity and structures of a rationally designed prefusion
724 MERS-CoV spike antigen. Proc Natl Acad Sci U S A *114*, E7348-E7357. 10.1073/pnas.1707304114.
725 PHE (2021). Investigation of novel SARS-CoV-2 variant Variant of Concern 202012/01 Technical briefing
726 5.
727 Polack, F.P., Thomas, S.J., Kitchin, N., Absalon, J., Gurtman, A., Lockhart, S., Perez, J.L., Pérez Marc, G.,
728 Moreira, E.D., Zerbini, C., et al. (2020). Safety and Efficacy of the BNT162b2 mRNA Covid-19 Vaccine. N
729 Engl J Med. 10.1056/NEJMoa2034577.
730 Ripperger, T.J., Uhrlaub, J.L., Watanabe, M., Wong, R., Castaneda, Y., Pizzato, H.A., Thompson, M.R.,
731 Bradshaw, C., Weinkauf, C.C., Bime, C., et al. (2020). Orthogonal SARS-CoV-2 Serological Assays Enable
732 Surveillance of Low-Prevalence Communities and Reveal Durable Humoral Immunity. Immunity *53*, 925-
733 933.e924. 10.1016/j.immuni.2020.10.004.
734 Robbiani, D.F., Gaebler, C., Muecksch, F., Lorenzi, J.C.C., Wang, Z., Cho, A., Agudelo, M., Barnes, C.O.,
735 Gazumyan, A., Finkin, S., et al. (2020). Convergent antibody responses to SARS-CoV-2 in convalescent
736 individuals. Nature *584*, 437-442. 10.1038/s41586-020-2456-9.
737 Rodda, L.B., Netland, J., Shehata, L., Pruner, K.B., Morawski, P.A., Thouvenel, C.D., Takehara, K.K.,
738 Eggenberger, J., Hemann, E.A., Waterman, H.R., et al. (2021). Functional SARS-CoV-2-Specific Immune
739 Memory Persists after Mild COVID-19. Cell *184*, 169-183.e117. 10.1016/j.cell.2020.11.029.
740 Saphire, E.O., Schendel, S.L., Fusco, M.L., Gangavarapu, K., Gunn, B.M., Wec, A.Z., Halfmann, P.J.,
741 Brannan, J.M., Herbert, A.S., Qiu, X., et al. (2018). Systematic Analysis of Monoclonal Antibodies against
742 Ebola Virus GP Defines Features that Contribute to Protection. Cell *174*, 938-952.e913.
743 10.1016/j.cell.2018.07.033.
744 Schäfer, A., Muecksch, F., Lorenzi, J.C.C., Leist, S.R., Cipolla, M., Bournazos, S., Schmidt, F., Maison, R.M.,
745 Gazumyan, A., Martinez, D.R., et al. (2021). Antibody potency, effector function, and combinations in
746 protection and therapy for SARS-CoV-2 infection in vivo. J Exp Med *218*. 10.1084/jem.20201993.
747 Seow, J., Graham, C., Merrick, B., Acors, S., Pickering, S., Steel, K.J.A., Hemmings, O., O'Byrne, A.,
748 Kouphou, N., Galao, R.P., et al. (2020). Longitudinal observation and decline of neutralizing antibody
749 responses in the three months following SARS-CoV-2 infection in humans. Nat Microbiol *5*, 1598-1607.
750 10.1038/s41564-020-00813-8.

751 Shinde, V., Bhikha, S., Hossain, Z., Archary, M., Bhorat, Q., Fairlie, L., Lalloo, U., Masilela, M.L.S.,
752 Moodley, D., Hanley, S., et al. (2021). Preliminary Efficacy of the NVX-CoV2373 Covid-19 Vaccine Against
753 the B.1.351 Variant. medRxiv, 2021.2002.2025.21252477. 10.1101/2021.02.25.21252477.
754 Smith, K., Garman, L., Wrammert, J., Zheng, N.Y., Capra, J.D., Ahmed, R., and Wilson, P.C. (2009). Rapid
755 generation of fully human monoclonal antibodies specific to a vaccinating antigen. Nat Protoc *4*, 372-
756 384. 10.1038/nprot.2009.3.
757 Song, G., He, W.T., Callaghan, S., Anzanello, F., Huang, D., Ricketts, J., Torres, J.L., Beutler, N., Peng, L.,
758 Vargas, S., et al. (2020). Cross-reactive serum and memory B cell responses to spike protein in SARS-CoV-
759 2 and endemic coronavirus infection. bioRxiv. 10.1101/2020.09.22.308965.
760 Stadlbauer, D., Amanat, F., Chromikova, V., Jiang, K., Strohmeier, S., Arunkumar, G.A., Tan, J., Bhavsar,
761 D., Capuano, C., Kirkpatrick, E., et al. (2020). SARS-CoV-2 Seroconversion in Humans: A Detailed Protocol
762 for a Serological Assay, Antigen Production, and Test Setup. Curr Protoc Microbiol *57*, e100.
763 10.1002/cpmc.100.
764 Stuart, T., Butler, A., Hoffman, P., Hafemeister, C., Papalexi, E., Mauck, W.M., Hao, Y., Stoeckius, M.,
765 Smibert, P., and Satija, R. (2019). Comprehensive Integration of Single-Cell Data. Cell *177*, 1888-
766 1902.e1821. 10.1016/j.cell.2019.05.031.
767 Sun, W., Leist, S.R., McCroskery, S., Liu, Y., Slamanig, S., Oliva, J., Amanat, F., Schafer, A., Dinnon, K.H.,
768 3rd, Garcia-Sastre, A., et al. (2020). Newcastle disease virus (NDV) expressing the spike protein of SARS-
769 CoV-2 as a live virus vaccine candidate. EBioMedicine *62*, 103132. 10.1016/j.ebiom.2020.103132.
770 Tegally, H., Wilkinson, E., Giovanetti, M., Iranzadeh, A., Fonseca, V., Giandhari, J., Doolabh, D., Pillay, S.,
771 San, E.J., Msomi, N., et al. (2020). Emergence and rapid spread of a new severe acute respiratory
772 syndrome-related coronavirus 2 (SARS-CoV-2) lineage with multiple spike mutations in South Africa.
773 medRxiv, 2020.2012.2021.20248640. 10.1101/2020.12.21.20248640.
774 Thomson, E.C., Rosen, L.E., Shepherd, J.G., Spreafico, R., da Silva Filipe, A., Wojcechowskyj, J.A., Davis,
775 C., Piccoli, L., Pascall, D.J., Dillen, J., et al. (2021). Circulating SARS-CoV-2 spike N439K variants maintain
776 fitness while evading antibody-mediated immunity. Cell. 10.1016/j.cell.2021.01.037.
777 Turner, J.S., Zhou, J.Q., Han, J., Schmitz, A.J., Rizk, A.A., Alsoussi, W.B., Lei, T., Amor, M., McIntire, K.M.,
778 Meade, P., et al. (2020). Human germinal centres engage memory and naive B cells after influenza
779 vaccination. Nature *586*, 127-132. 10.1038/s41586-020-2711-0.
780 Wajnberg, A., Amanat, F., Firpo, A., Altman, D.R., Bailey, M.J., Mansour, M., McMahon, M., Meade, P.,
781 Mendu, D.R., Muellers, K., et al. (2020). Robust neutralizing antibodies to SARS-CoV-2 infection persist
782 for months. Science *370*, 1227-1230. 10.1126/science.abd7728.
783 Walsh, E.E., Frenck, R., Falsey, A.R., Kitchin, N., Absalon, J., Gurtman, A., Lockhart, S., Neuzil, K., Mulligan,
784 M.J., Bailey, R., et al. (2020). RNA-Based COVID-19 Vaccine BNT162b2 Selected for a Pivotal Efficacy
785 Study. medRxiv, 2020.2008.2017.20176651. 10.1101/2020.08.17.20176651.
786 Wang, Z., Schmidt, F., Weisblum, Y., Muecksch, F., Barnes, C.O., Finkin, S., Schaefer-Babajew, D., Cipolla,
787 M., Gaebler, C., Lieberman, J.A., et al. (2021). mRNA vaccine-elicited antibodies to SARS-CoV-2 and
788 circulating variants. Nature. 10.1038/s41586-021-03324-6.
789 Weisblum, Y., Schmidt, F., Zhang, F., DaSilva, J., Poston, D., Lorenzi, J.C., Muecksch, F., Rutkowska, M.,
790 Hoffmann, H.H., Michailidis, E., et al. (2020). Escape from neutralizing antibodies by SARS-CoV-2 spike
791 protein variants. Elife *9*. 10.7554/eLife.61312.
792 Wibmer, C.K., Ayres, F., Hermanus, T., Madzivhandila, M., Kgagudi, P., Lambson, B.E., Vermeulen, M.,
793 van den Berg, K., Rossouw, T., Boswell, M., et al. (2021). SARS-CoV-2 501Y.V2 escapes neutralization by
794 South African COVID-19 donor plasma. bioRxiv, 2021.2001.2018.427166. 10.1101/2021.01.18.427166.
795 Wilson, P., Stamper, C., Dugan, H., Li, L., Asby, N., Halfmann, P., Guthmiller, J., Zheng, N.Y., Huang, M.,
796 Stovicek, O., et al. (2020). Distinct B cell subsets give rise to antigen-specific antibody responses against
797 SARS-CoV-2. Res Sq. 10.21203/rs.3.rs-80476/v1.

798 Wohlbold, T.J., Chromikova, V., Tan, G.S., Meade, P., Amanat, F., Comella, P., Hirsh, A., and Krammer, F.
799 (2016). Hemagglutinin Stalk- and Neuraminidase-Specific Monoclonal Antibodies Protect against Lethal
800 H10N8 Influenza Virus Infection in Mice. J Virol *90*, 851-861. 10.1128/JVI.02275-15.
801 Wohlbold, T.J., Nachbagauer, R., Xu, H., Tan, G.S., Hirsh, A., Brokstad, K.A., Cox, R.J., Palese, P., and
802 Krammer, F. (2015). Vaccination with adjuvanted recombinant neuraminidase induces broad
803 heterologous, but not heterosubtypic, cross-protection against influenza virus infection in mice. mBio *6*,
804 e02556. 10.1128/mBio.02556-14.
805 Wrammert, J., Koutsonanos, D., Li, G.M., Edupuganti, S., Sui, J., Morrissey, M., McCausland, M.,
806 Skountzou, I., Hornig, M., Lipkin, W.I., et al. (2011). Broadly cross-reactive antibodies dominate the
807 human B cell response against 2009 pandemic H1N1 influenza virus infection. J Exp Med *208*, 181-193.
808 jem.20101352 [pii]

809 10.1084/jem.20101352.

810 Wrammert, J., Smith, K., Miller, J., Langley, W.A., Kokko, K., Larsen, C., Zheng, N.Y., Mays, I., Garman, L.,
811 Helms, C., et al. (2008). Rapid cloning of high-affinity human monoclonal antibodies against influenza
812 virus. Nature 4*53,* 667-671. 10.1038/nature06890.
813 Wrapp, D., Wang, N., Corbett, K.S., Goldsmith, J.A., Hsieh, C.L., Abiona, O., Graham, B.S., and McLellan,
814 J.S. (2020). Cryo-EM structure of the 2019-nCoV spike in the prefusion conformation. Science.
815 10.1126/science.abb2507.
816 Wu, K., Werner, A.P., Moliva, J.I., Koch, M., Choi, A., Stewart-Jones, G.B.E., Bennett, H., Boyoglu-Barnum,
817 S., Shi, W., Graham, B.S., et al. (2021). mRNA-1273 vaccine induces neutralizing antibodies against spike
818 mutants from global SARS-CoV-2 variants. bioRxiv, 2021.2001.2025.427948.
819 10.1101/2021.01.25.427948.
820 Ye, J., Ma, N., Madden, T.L., and Ostell, J.M. (2013). IgBLAST: an immunoglobulin variable domain
821 sequence analysis tool. Nucleic Acids Res 4*1,* W34-40. 10.1093/nar/gkt382.
822

823 **Figure Legends**

824 **Figure 1: Antibody responses in individuals vaccinated with mRNA-based SARS-CoV-2 vaccines.**
825 Antibody responses of convalescent individuals and vaccinees to full length spike protein (**A**) and RBD (**B**)
826 as measured by ELISA and neutralizing activity of the sera of the same individuals in a microneutralization
827 assay against authentic SARS-CoV-2 (**C)**. Convalescent individuals were grouped based on their initial
828 antibody response (measured in a CLIA laboratory) to spike protein into +, ++, and +++. **D** shows ratios
829 between binding and neutralizing antibody levels in vaccinees and convalescent individuals. Higher ratios
830 indicate a bias towards non-neutralizing antibodies. **E, F, G and H** show antibody responses against α-
831 coronavirus 229E and NL63 and β-coronavirus OC43 and HKU1 spike proteins over time.

832

833 **Figure 2. Characterization of mAbs derived from vaccine plasmablasts**. Binding of plasmablasts derived
834 from three vaccinees (V3, V5 and V6) against full length spike (**A**), RBD (**B**), NTD (**C**) and S2 (**D**). **E** shows
835 the percentages of the respective antibodies per subject. **F** shows neutralizing activity of the mABs against
836 authentic SARS-CoV-2 and the proportion of neutralizing antibodies per subject is shown in **G**. **H and I**
837 show reactivity of mAbs to spike protein of human β-coronaviruses OC43 and HKU1. MBC = minimal
838 binding concentration.

839

840 **Figure 3. Characterization of bulk sorted plasmablasts via single-cell RNA sequencing. (A)** Uniform
841 manifold approximation and projection (UMAP) of scRNAseq from bulk plasmablast with recovered BCR
842 sequences (purple) or unrecovered (grey). **(B)** UMAP overlay of percent of cellular population expressing
843 *MZB1*, *PRDM1*, and *XPB1*. Hexbin equals 80 individual cells. (**C**) UMAP overlay of BCR sequences with
844 confirmed spike binding activity. (**D**) Proportional composition of heavy chains genes in the spike binding
845 sequences broken down by sample. **(E)** Comparison of nucleotide-level mutation frequency in
846 immunoglobulin heavy chain variable (IGHV) genes between plasmablasts clonally related to spike binding
847 mAbs from SARS-CoV-2 vaccinees, plasmablasts sorted from PBMCs one week after seasonal influenza
848 vaccination and found in vaccine-responding B cell clones, and naïve B cells found in blood of an influenza
849 vaccinee (left panel); and between plasmablasts from SARS-CoV-2 vaccinees found to be clonally related
850 to spike-binding mAbs that were, respectively, cross-reactive and non-cross-reactive to human β-
851 coronaviruses spike proteins (right panel).

852

853 **Figure 4. Mapping of the amino-acid substitutions and deletions onto the structure of the SARS-CoV-2**
854 **spike glycoprotein. A** lists mutations of the three major variants of concern B.1.17, B.1.315 and P.1. **B**
855 shows these mutations mapped onto the structure of the spike glycoprotein (model generated by
856 superposition of PDB 6M0j and 7C2L (Chi *et al.*, 2020; Lan et al., 2020)). One RBD in the up conformation
857 (red) is bound with ACE2 receptor (pink). The NTD is colored blue and the various amino-acid substitutions
858 are shown as yellow spheres. One spike protomer is shown in bold colors while the other two are colored
859 white. **C** shows competition between ACE2 and neutralizing RBD targeting mAbs PVI.V3-9 and PVI.V6-4
860 for binding to RBD. **D** BLI- measured binding affinities of the RBD mutants to ACE2, as well as the calculated
861 fold change, are shown in the table on the right.

862

863 **Figure 5. Binding and neutralization of SARS-CoV-2 variants.** Binding of serum samples from convalescent
864 individuals, vaccinees and vaccine derived mAbs to a panel of RBD mutants is shown in **A, B and C**
865 respectively. The red line in A indicates the average reduction. Dotted lines in A and B indicate 100%, the
866 line with smaller dots in C indicated reactivity of the anti-his coating control. For vaccinees late samples
867 (V1=d89, V2=d102, V3=d47, V4=d48, V5=49 and V6=48) were assayed. **D** shows the spike mutations of
868 virus isolate PVI14252 modelled on a co-crystal structure of the SARS-CoV-2 spike protein with ACE2
869 (model generated by superposition of PDB 6M0j and 7C2L (Chi *et al.*, 2020; Lan *et al.*, 2020)). **E and F** show
870 the inhibitory effect of vaccine serum and vaccine derived neutralizing antibodies on both wild type SARS-
871 CoV-2 and PV14252. **G** shows neutralizing activity of the plasmablast derived neutralizing antibodies
872 aginst wild type, B.1.1.7 and B.1.351 virus isolates. Of note, these comparative assays were always
873 performed side by side but sets are run by different operators and on a different Vero cell clone as the
874 neutralization assays shown in Figure 2.

875

876

877 **Supplemental Table 1: Study participant and biospecimen information**

Vaccinees	Spike IgG response[1*]	Sex	Age group (yrs)	Specimen tested

V1	Strong positive	F	>60	several longitudinal time points including days 34, 68, 89 and 188 post vaccination
V2	Strong positive	M	30-40	several longitudinal time points including days 19, 47, 74, 102, 129, 157 and 186 post vaccination
V3	Strong positive	F	50-60	several longitudinal time points including days 19, 27, 47, 77 and 102 post vaccination
V4	Strong positive	M	>60	several longitudinal time points including days 27, 48 and 89 post vaccination
V5	Strong positive	F	40-50	several longitudinal time points including 27, 49 and 83 days post vaccination
V6	Strong positive	F	30-40	several longitudinal time points including 27, 48 and 83 days post vaccination
Seronegative, post pandemic		**Sex**	**Age group (yrs)**	**Days from last negative serology test when the sample was taken**
N1	Negative	F	40-50	23
N2	Negative	F	20-29	24
N3	Negative	F	20-29	23
N4	Negative	F	30-35	22
Seropositive, natural infection		**Sex**	**Age group (yrs)**	**Days post onset of COVID-19 symptoms when the sample was taken**
P1	Weak positive	M	20-29	260
P2	Weak positive	M	50-59	no data available
P3	Weak positive	F	30-39	111
P4	Weak positive	F	30-39	221

P5	Weak positive	F	30-39	254
P6	Weak positive	F	20-29	247
P7	Weak positive	M	30-39	220
P8	Weak positive	F	20-29	Asymptomatic
P9	Moderate positive	M	30-39	no data available
P10	Moderate positive	F	30-39	197
P11	Moderate positive	F	50-59	Asymptomatic
P12	Moderate positive	F	30-39	Asymptomatic
P13	Moderate positive	M	30-39	234
P14	Moderate positive	F	20-29	273
P15	Moderate positive	M	30-39	Asymptomatic
P16	Moderate positive	F	20-29	258
P17	Moderate positive	F	20-29	246
P18	Moderate positive	M	20-29	Asymptomatic
P19	Moderate positive	F	50-59	204
P20	Strong positive	F	50-59	no data available
P21	Strong positive	F	30-39	245
P22	Strong positive	M	NA	170
P23	Strong positive	F	>60	Asymptomatic
P24	Strong positive	F	40-49	no data available
P25	Strong positive	F	50-59	191
P26	Strong positive	F	30-39	no data available
P27	Strong positive	F	50-59	113
P28	Strong positive	M	>60	Asymptomatic
P29	Strong positive	M	18-19	218
P30	Strong positive	M	50-59	219

878 [1]Samples were categorized based on initial titers obtained from Mount Sinai's CLIA laboratory test. Weak
879 positive: 1:80 – 1:160 weak positive; 1:320-1:960 moderate positive; 1:960-1: ≥2880 strong positive

880 * All six vaccinees were sero-negative for SARS-CoV-2 without clinical evidence of COVID10 prior to SARS-
881 CoV-2 spike mRNA vaccination.

882

883 **Supplemental Table 2: Immunoglobulin gene usage of the spike-mAbs**

Name	Native isotype	Heavy chain		Light chain	
		Gene usage	HCDR3 AA sequence	Gene usage	LCDR3 AA sequence
PVI.V5-1	IgG1	VH3-23 DH5-18 JH4	CAPHRGQLWFDYW	VK3-20 JK4	CQQYGSSPPTF
PVI.V5-2	IgG1	VH3-21 DH2-2 JH4	CARDLKLSPAAIGWDYFDYW	VK3-15 JK2	CQQYNNWPRSF
PVI.V5-3	IgG1	VH3-7 DH6-13 JH4	CAIFGAAGTDYW	VL3-16 JL3	CLSADSSGTYWVF
PVI.V5-4	IgG1	VH3-30 DH3-22 JH4	CARENNYYDSSGYSYYFDYW	VK3-20 JK2	CQQYGSSPMCSF
PVI.V5-5	IgA1	VH1-69 DH5-24 JH4	CARDFGREWLQYFYFDCW	VK3-20 JK4	CQQYGSSPTF

PVI.V5-6	IgG1	VH3-7 DH3-3 JH4	CARDNNDFWSGYLYFDYW	VL3-10 JL2	CYSTDSSGNHRGVF
PVI.V6-1	IgG1	VH3-30 DH6-19 JH4	CARGAVAGQHSFDNW	VK2-30 JK4	CMQGTHWPPTF
PVI.V6-2	IgG1	VH3-33 DH6-13 JH4	CARDKRGSSSWLDQYFDYW	VL3-21 JL2	CQVWDSSSDHVVF
PVI.V6-3	IgG1	VH4-31 DH3-22 JH5	CARDMISGRGLFDPW	VK1-33 JK2	CQQYDNLPTF
PVI.V6-4	IgG1	VH1-69 DH4-17 JH3	CARGNYDYGDYLLKGSAFDIW	VK4-1 JK2	CQQYYSTPPNTF
PVI.V6-5	IgG1	VH3-30 DH3-10 JH4	CAKDGGYYYYGSGSYPSYFDYW	VK2D-29 JK4	CMQSIQLPLTF
PVI.V6-6	IgG1	VH4-31 DH3-10 JH6	CASEKFLWGQGYYYGMDVW	VL2-14 JL2	CSSYTSSSTLVF
PVI.V6-7	IgG1	VH4-39 DH3-22 JH4	CATQSDYDSSGLEFDYW	VL2-14 JL3	CSSYTSSSSWVF
PVI.V6-8	IgG1	VH4-31 DH3-22 JH3	CARGREEPIVVVTDAFDIW	VK3-11 JK2	CQQRSNWPPMYTF
PVI.V6-9	IgG1	VH3-30 DH2-15 JH4	CAKSGYPYCGGGTCYSGWFDYW	VK1-33 JK2	CQRYDNPPYTF
PVI.V6-10	IgG1	VH1-2 DH6-19 JH6	CAREIAVAGNDYSYGLDVW	VK3-20 JK4	CQQYGSSLLTF
PVI.V6-11	IgG1	VH1-46 DH6-19 JH6	CASQSHWQWLGGGDSYGMDVW	VK1-9 JK2	CQQLNSYPYTF
PVI.V6-12	IgG1	VH5-51 DH1-26 JH4	CARRFGSYPPYFDYW	VL3-21 JL1	CQVWDSNSDLYVF
PVI.V6-13	IgG1	VH3-30 DH5-18 JH4	CAKAGYSYAYGDYYFDYW	VK1-33 JK3	CQHYDNLPPAVTF
PVI.V6-14	IgG1	VH4-39 DH3-10 JH4	CARCRPEYYFGSGSYLDFDYW	VK1-12 JK4	CQQANSFPLTF
PVI.V6-15	IgG1	VH3-30 DH5-18 JH4	CAKDWGWIQLWGLDYW	VL2-18 JL3	CSSYTSSSTWVF
PVI.V3-1	IgG1	VH4-4 DH1-26 JH4	CVSRGVGATREKDYW	VK3-15 JK4	CQQYNNWPPDLTF
PVI.V3-2	IgG1	VH4-39 DH3-10 JH4	CASLDYYGSGSGPGYFDYW	VK3-11 JK4	CQQRSNWLTF
PVI.V3-3	IgG3	VH3-33 DH6-19 JH4	CASDSSGWYYFDYW	VL3-9 JL2	CQVWDSSTVVF
PVI.V3-4	IgG1	VH3-21 DH2-21 JH3	CAVTLLPTYCGGEWCAFDIW	VK3-15 JK2	CQQYNNWPPYTF
PVI.V3-5	IgG1	VH1-69 DH3-22 JH4	CARNYYDSSGSQGMDYW	VK3-11 JK4	CQQRSNWPPVLTF
PVI.V3-6	IgA1	VH3-66 DH3-3 JH4	CARHLGVVI[1]	VK4-1 JK1	CQQYYSTLWTF
PVI.V3-7	IgG3	VH4-39 DH1-26 JH4	CAKPSGSYLGFDYW	VK1-39 JK3	CQQSYSTPFTF
PVI.V3-8	IgG1	VH4-38 DH3-3 JH4	CARSDFSVRVGFDCW	VK4-1 JK2	CQQSYTTNTF
PVI.V3-9	IgG1	VH3-53 DH3-16 JH6	CARDLMEGGGMDVW	VK3-20 JK1	CQQYGSSLGTF
PVI.V3-10	IgG1	VH4-34 DH3-22 JH4	CARSQPLLWSSGYCCDYW	VL2-11 JL2	CCSYAGSYTLVF
PVI.V3-11	IgG1	VH3-64D DH4-11 JH4	CVRGPTVTTENDFDSW	VK2-30 JK2	CMQGTHSYTF
PVI.V3-12	IgG2	VH1-46 DH5-24 JH4	CASDPNRDGLALDSW	VK3-20 JK2	CQQYGTSPLYTF
PVI.V3-13	IgG1	VH1-69 DH1-14 JH4	CARDRYHGSPVDYW	VK3-11 JK4	CQQRSNWPPSLTF
PVI.V3-14	IgG1	VH4-31 DH5-12 JH4	CARARYSGSARGPPKQYYFDYW	VK3-20 JK1	CQHLVTF
PVI.V3-15	IgG1	VH3-21 DH3-3 JH3	CARDGGRGYDFWSGYYIGAFDIW	VK3-15 JK4	CQQYNDWPPLTF
PVI.V3-16	IgG1	VH3-33 DH2-15 JH6	CARGLGWDIVVVVSGEMDGMDVW	VL1-40 JL1	CQSYDSSLSGPYVF
PVI.V3-17	IgA1	VH3-20 DH2-2 JH4	CARGEGSSDYW	VK3-20 JK1	CQQYGSSPKTF
PVI.V3-18	IgG1	VH3-30 DH2-15 JH4	CAKASGLYCSGGNCLVADFDYW	VL1-39 JL4	CQQSYSTPLSF
PVI.V3-19	IgG1	VH5-51 DH6-19 JH6	CARRNTSAQYSSGWYVHYYYGMDVW	VK2-28 JK3	CMQALQTPGFTF
PVI.V3-20	IgG1	VH3-30 DH3-3 JH6	CAKDQLGAIFAHYYYYGMDVW	VL1-40 JL1	CQSYDSSLSGYVF
PVI.V3-21	IgG1	VH5-51 DH5-24 JH4	CAKLSRDAYRGPFDYW	VL6-57 JL2	CQSYDSSNPDVVF

[1]Indicates absence of the W118 residue from the junction of the CDR3.

Supplementary Figure 1. **Full length spike to RBD ratios (A) and comparison of binding to neutralizing titer ratios between naturally infected and vaccinated individuals (B).**

Supplementary Figure 2. **Gating strategy for sorting plasmablasts from total PBMCs isolated one week after second immunization.**

Supplementary Figure 3. Representative Biolayer Interferometry binding isotherms from two independent experiments. The raw data are show in pink and the Langmuir 1:1 kinetics fit is show in black.

895

896 **Supplementary Figure 4. Binding of SARS-CoV-2 variant RBDs to ACE2. A.** ELISA curves of the RBD variants
897 binding to human ACE2. Shown are the binding curves calculated with nonlinear regression to the
898 arithmetic mean values from eight replicates ± SEM. The calculated steady-state K_D values ± SEM from
899 end-point ELISA measurements and the fold-change in comparison to wild type RBD are reported in **B.**

900

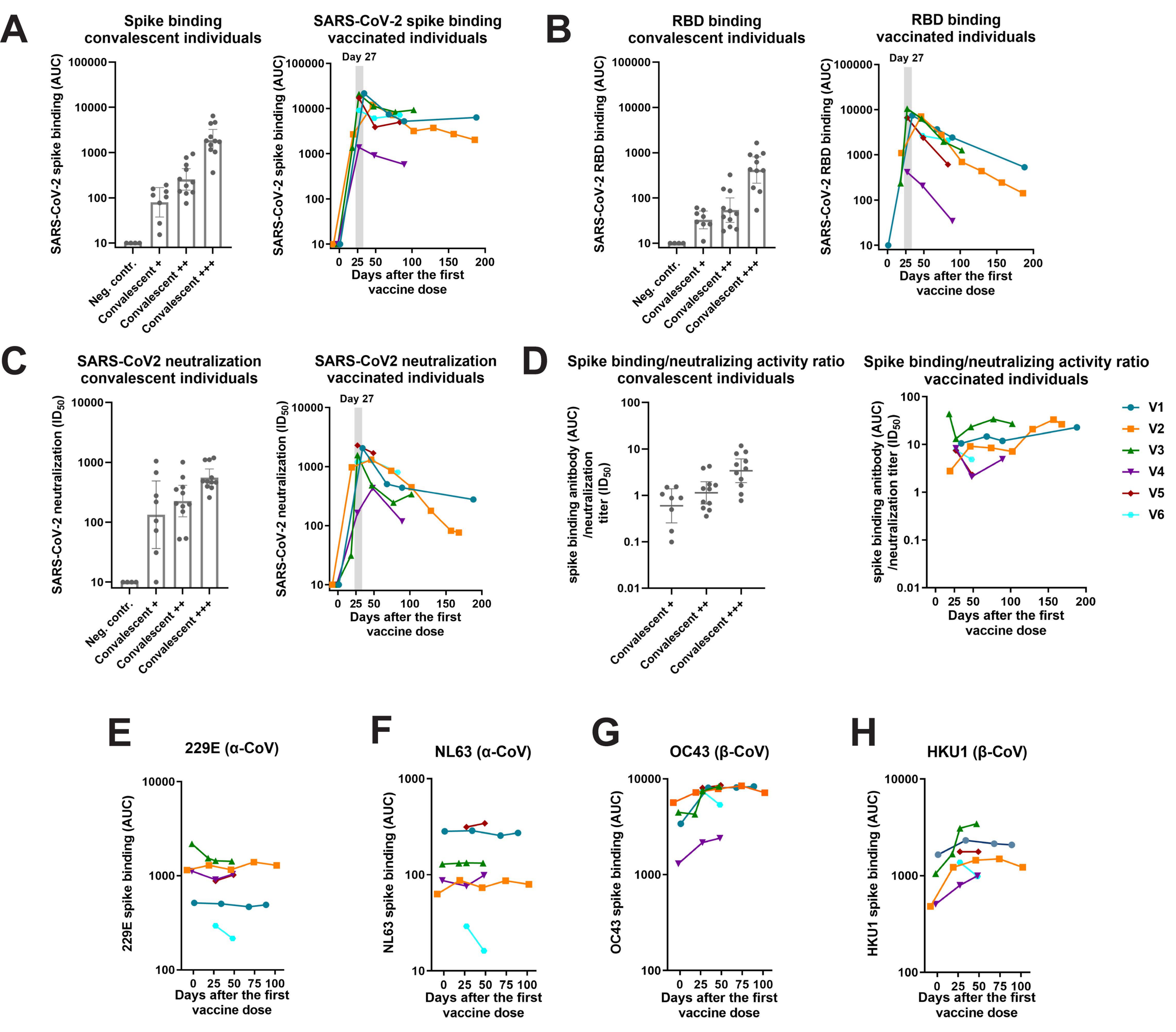
A
Spike binding convalescent individuals
SARS-CoV-2 spike binding (AUC)
Neg. contr.
Convalescent +
Convalescent ++
Convalescent +++
SARS-CoV-2 spike binding vaccinated individuals
Day 27
Days after the first vaccine dose
B
RBD binding convalescent individuals
SARS-CoV-2 RBD binding (AUC)
RBD binding vaccinated individuals
C
SARS-CoV2 neutralization convalescent individuals
SARS-CoV-2 neutralization (ID50)
SARS-CoV2 neutralization vaccinated individuals
D
Spike binding/neutralizing activity ratio convalescent individuals
spike binding anitbody (AUC) /neutralization titer (ID50)
Spike binding/neutralizing activity ratio vaccinated individuals
V1
V2
V3
V4
V5
V6
E
229E (α-CoV)
229E spike binding (AUC)
F
NL63 (α-CoV)
NL63 spike binding (AUC)
G
OC43 (β-CoV)
OC43 spike binding (AUC)
H
HKU1 (β-CoV)
HKU1 spike binding (AUC)

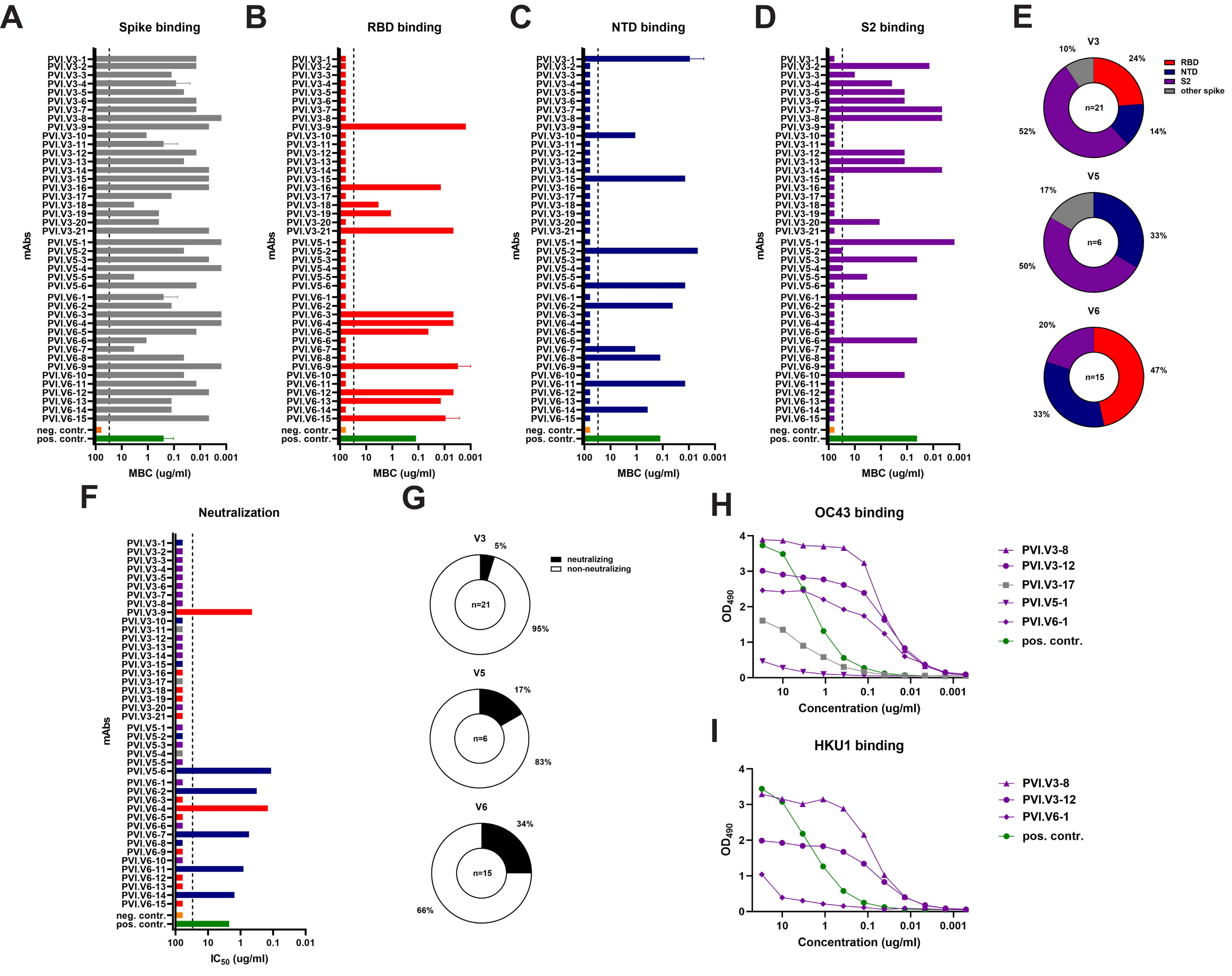
A
Spike binding
B
RBD binding
C
NTD binding
D
S2 binding
mAbs
PVI.V3-1
PVI.V3-2
PVI.V3-3
PVI.V3-4
PVI.V3-5
PVI.V3-6
PVI.V3-7
PVI.V3-8
PVI.V3-9
PVI.V3-10
PVI.V3-11
PVI.V3-12
PVI.V3-13
PVI.V3-14
PVI.V3-15
PVI.V3-16
PVI.V3-17
PVI.V3-18
PVI.V3-19
PVI.V3-20
PVI.V3-21
PVI.V5-1
PVI.V5-2
PVI.V5-3
PVI.V5-4
PVI.V5-5
PVI.V5-6
PVI.V6-1
PVI.V6-2
PVI.V6-3
PVI.V6-4
PVI.V6-5
PVI.V6-6
PVI.V6-7
PVI.V6-8
PVI.V6-9
PVI.V6-10
PVI.V6-11
PVI.V6-12
PVI.V6-13
PVI.V6-14
PVI.V6-15
neg. contr.
pos. contr.
100 10 1 0.1 0.01 0.001
MBC (ug/ml)
E
V3
10%
24%
52%
14%
n=21
RBD
NTD
S2
other spike
V5
17%
33%
50%
n=6
V6
20%
47%
33%
n=15
F
Neutralization
IC50 (ug/ml)
G
V3
5%
95%
n=21
neutralizing
non-neutralizing
V5
17%
83%
n=6
V6
34%
66%
n=15
H
OC43 binding
OD490
Concentration (ug/ml)
PVI.V3-8
PVI.V3-12
PVI.V3-17
PVI.V5-1
PVI.V6-1
pos. contr.
I
HKU1 binding
OD490
Concentration (ug/ml)
PVI.V3-8
PVI.V3-12
PVI.V6-1
pos. contr.

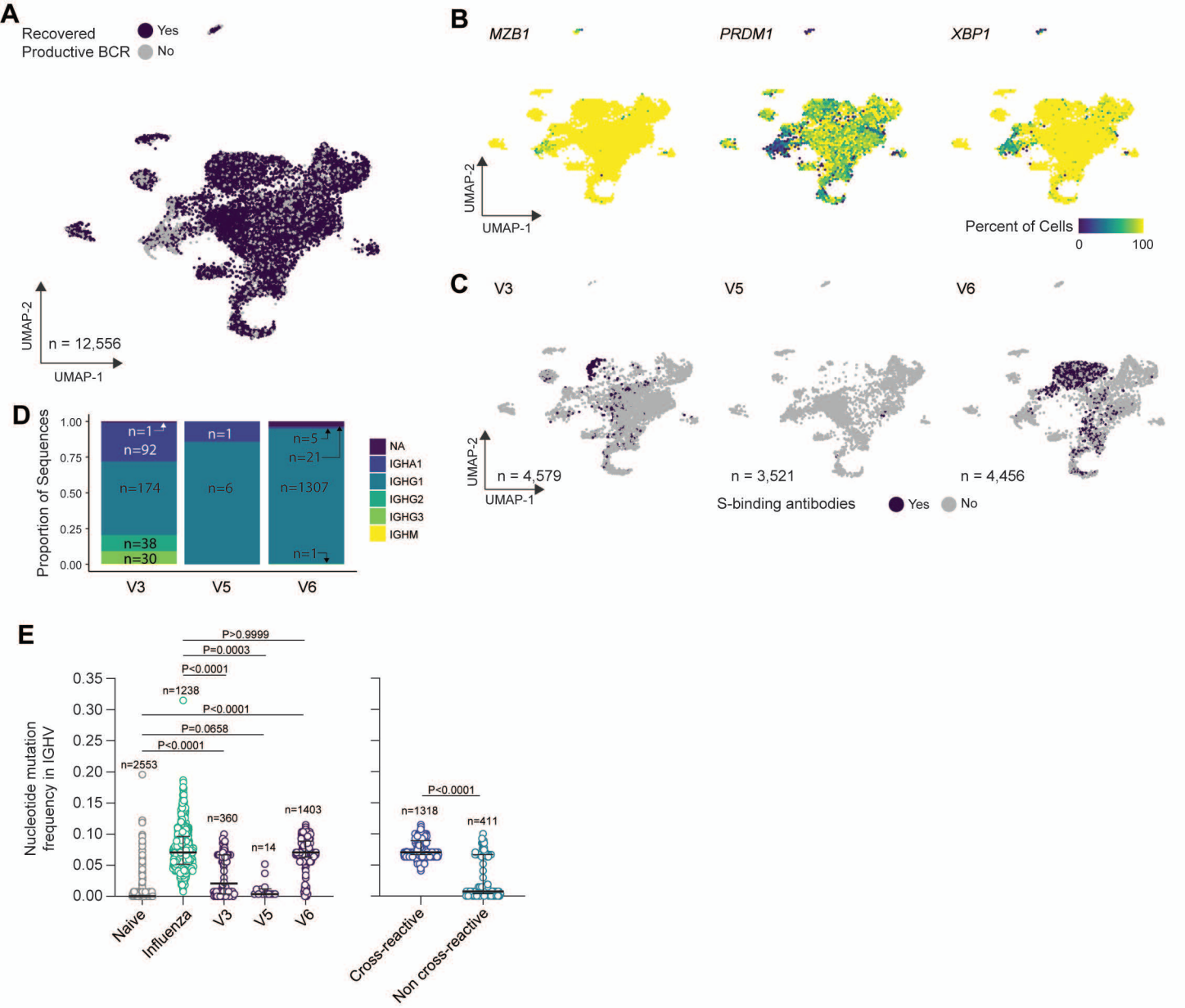
A
Recovered Productive BCR
Yes
No
UMAP-2
UMAP-1
n = 12,556
B
MZB1
PRDM1
XBP1
UMAP-2
UMAP-1
Percent of Cells
0
100
C
V3
V5
V6
UMAP-2
UMAP-1
n = 4,579
n = 3,521
n = 4,456
S-binding antibodies
Yes
No
D
Proportion of Sequences
1.00
0.75
0.50
0.25
0.00
n=1
n=92
n=174
n=38
n=30
n=1
n=6
n=5
n=21
n=1307
n=1
NA
IGHA1
IGHG1
IGHG2
IGHG3
IGHM
V3
V5
V6
E
Nucleotide mutation frequency in IGHV
0.35
0.30
0.25
0.20
0.15
0.10
0.05
0.00
P>0.9999
P=0.0003
P<0.0001
n=1238
P<0.0001
P=0.0658
P<0.0001
n=2553
n=360
n=14
n=1403
P<0.0001
n=1318
n=411
Naive
Influenza
V3
V5
V6
Cross-reactive
Non cross-reactive

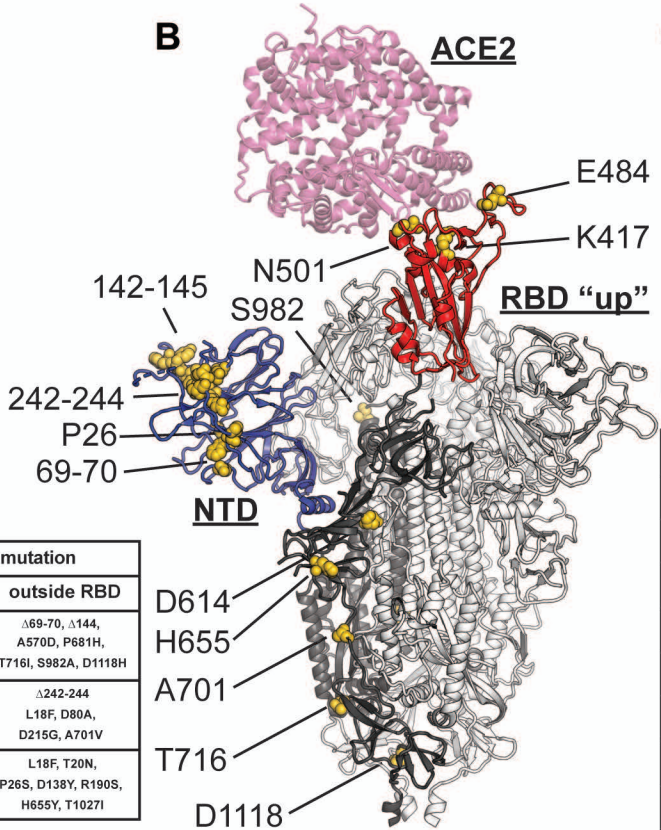

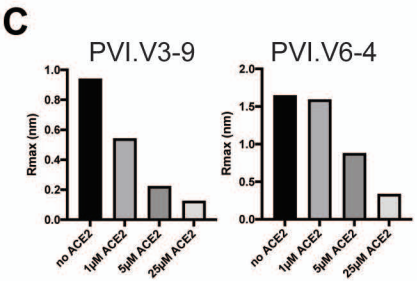

A

	spike mutation	
variant	RBD	outside RBD
B.1.1.7	N501Y	Δ69-70, Δ144, A570D, P681H, T716I, S982A, D1118H
B.1.351	K417N, E484K, N501Y	Δ242-244 L18F, D80A, D215G, A701V
P.1	K417T, E484K, N501Y	L18F, T20N, P26S, D138Y, R190S, H655Y, T1027I

D

RBD variant	K_D (nM)	Fold change
wild-type	35.4±5.6	1
N501Y	7.0±1.1	0.2
Y453F	29.9±18.1	0.8
N439K	15.7±3.8	0.4
Y453F/N439K	7.2±0.1	0.2
E484K	138.3±30.9	4
K417N/E484K/N501Y	34.0±4.6	1
K417T/E484K/N501Y	4.0±1.7	0.1

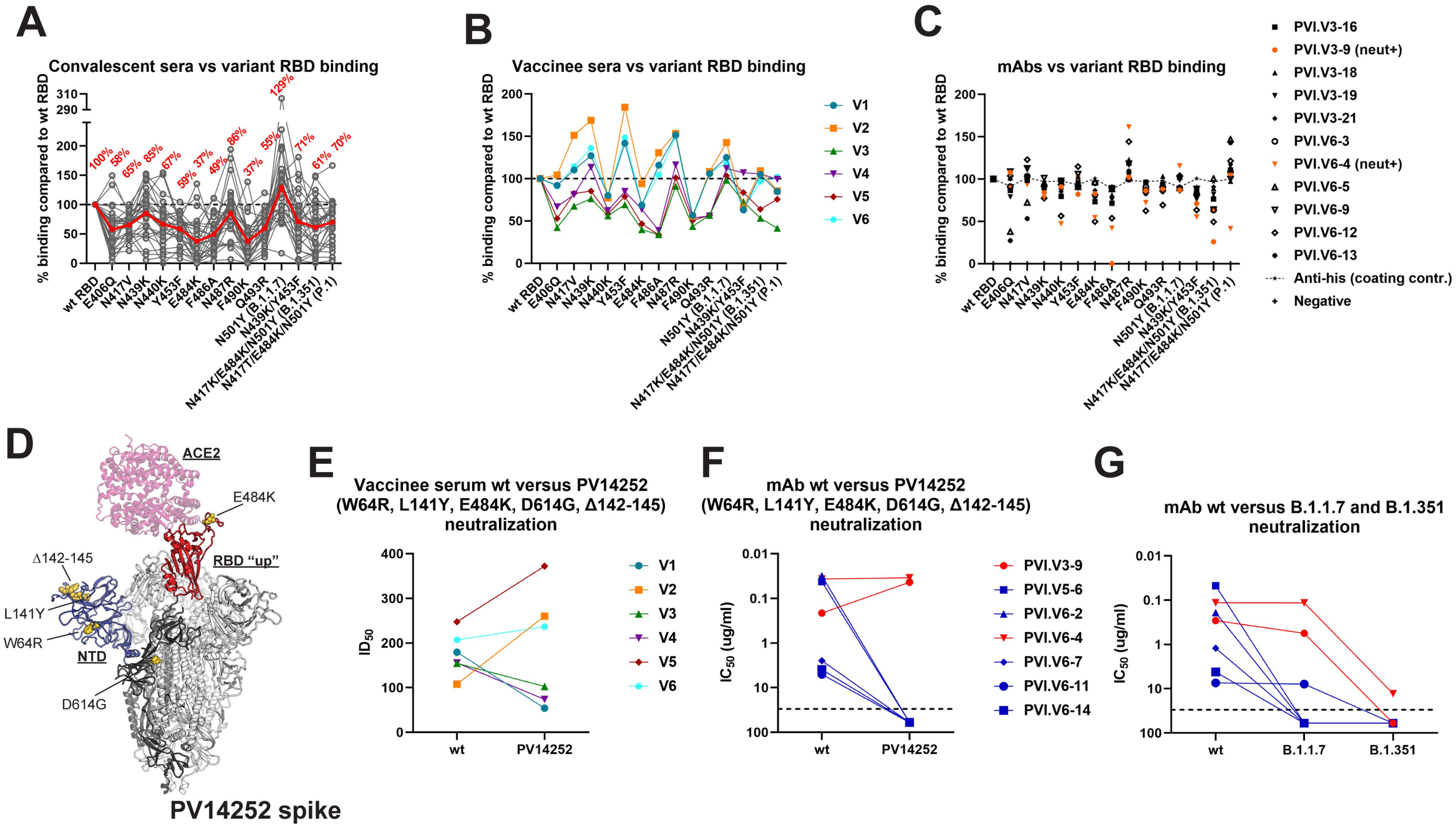
A
Convalescent sera vs variant RBD binding
% binding compared to wt RBD
100%
58%
65%
85%
67%
59%
37%
49%
86%
37%
55%
129%
71%
61%
70%
wt RBD
E406Q
N417V
N439K
N440K
Y453F
E484K
F486A
N487R
F490K
Q493R
N501Y (B.1.1.7)
N439K/Y453F
N417K/E484K/N501Y (B.1.351)
N417T/E484K/N501Y (P.1)
B
Vaccinee sera vs variant RBD binding
% binding compared to wt RBD
V1
V2
V3
V4
V5
V6
C
mAbs vs variant RBD binding
% binding compared to wt RBD
PVI.V3-16
PVI.V3-9 (neut+)
PVI.V3-18
PVI.V3-19
PVI.V3-21
PVI.V6-3
PVI.V6-4 (neut+)
PVI.V6-5
PVI.V6-9
PVI.V6-12
PVI.V6-13
Anti-his (coating contr.)
Negative
D
ACE2
E484K
Δ142-145
RBD "up"
L141Y
W64R
NTD
D614G
PV14252 spike
E
Vaccinee serum wt versus PV14252
(W64R, L141Y, E484K, D614G, Δ142-145)
neutralization
ID50
wt
PV14252
V1
V2
V3
V4
V5
V6
F
mAb wt versus PV14252
(W64R, L141Y, E484K, D614G, Δ142-145)
neutralization
IC50 (ug/ml)
wt
PV14252
PVI.V3-9
PVI.V5-6
PVI.V6-2
PVI.V6-4
PVI.V6-7
PVI.V6-11
PVI.V6-14
G
mAb wt versus B.1.1.7 and B.1.351
neutralization
IC50 (ug/ml)
wt
B.1.1.7
B.1.351

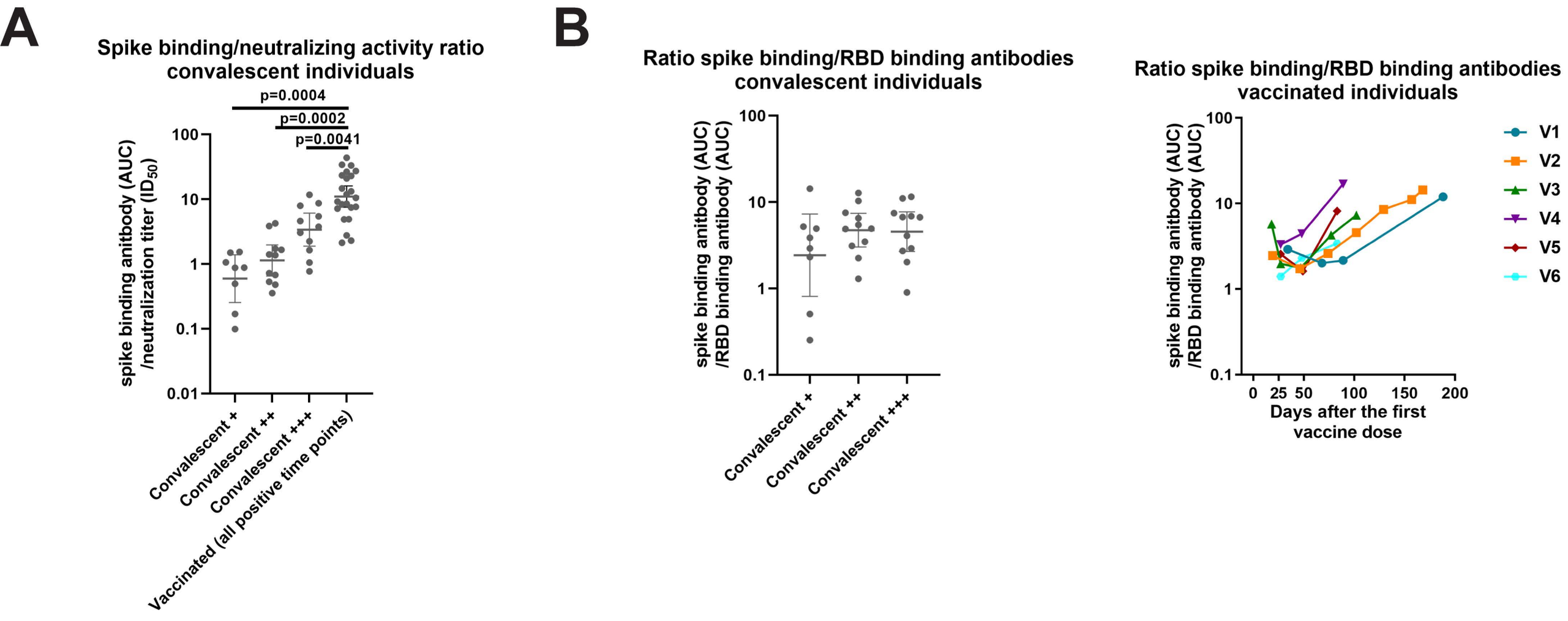
A
Spike binding/neutralizing activity ratio
convalescent individuals
p=0.0004
p=0.0002
p=0.0041
spike binding anitbody (AUC)
/neutralization titer (ID50)
100
10
1
0.1
0.01
Convalescent +
Convalescent ++
Convalescent +++
Vaccinated (all positive time points)
B
Ratio spike binding/RBD binding antibodies
convalescent individuals
spike binding anitbody (AUC)
/RBD binding antibody (AUC)
100
10
1
0.1
Convalescent +
Convalescent ++
Convalescent +++
Ratio spike binding/RBD binding antibodies
vaccinated individuals
spike binding anitbody (AUC)
/RBD binding antibody (AUC)
100
10
1
0.1
0
25
50
100
150
200
Days after the first
vaccine dose
V1
V2
V3
V4
V5
V6

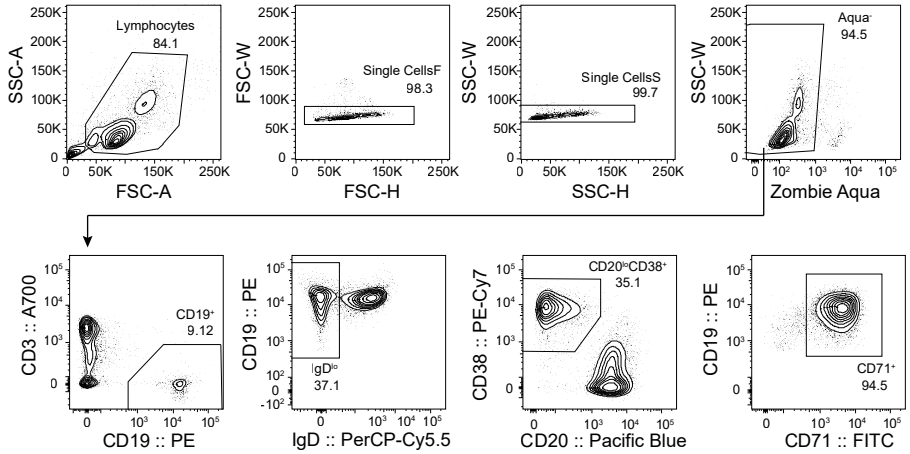
Lymphocytes
84.1
SSC-A
FSC-A
Single CellsF
98.3
FSC-W
FSC-H
Single CellsS
99.7
SSC-W
SSC-H
Aqua-
94.5
SSC-W
Zombie Aqua
CD19+
9.12
CD3 :: A700
CD19 :: PE
IgD-
37.1
CD19 :: PE
IgD :: PerCP-Cy5.5
CD20-CD38+
35.1
CD38 :: PE-Cy7
CD20 :: Pacific Blue
CD71+
94.5
CD19 :: PE
CD71 :: FITC

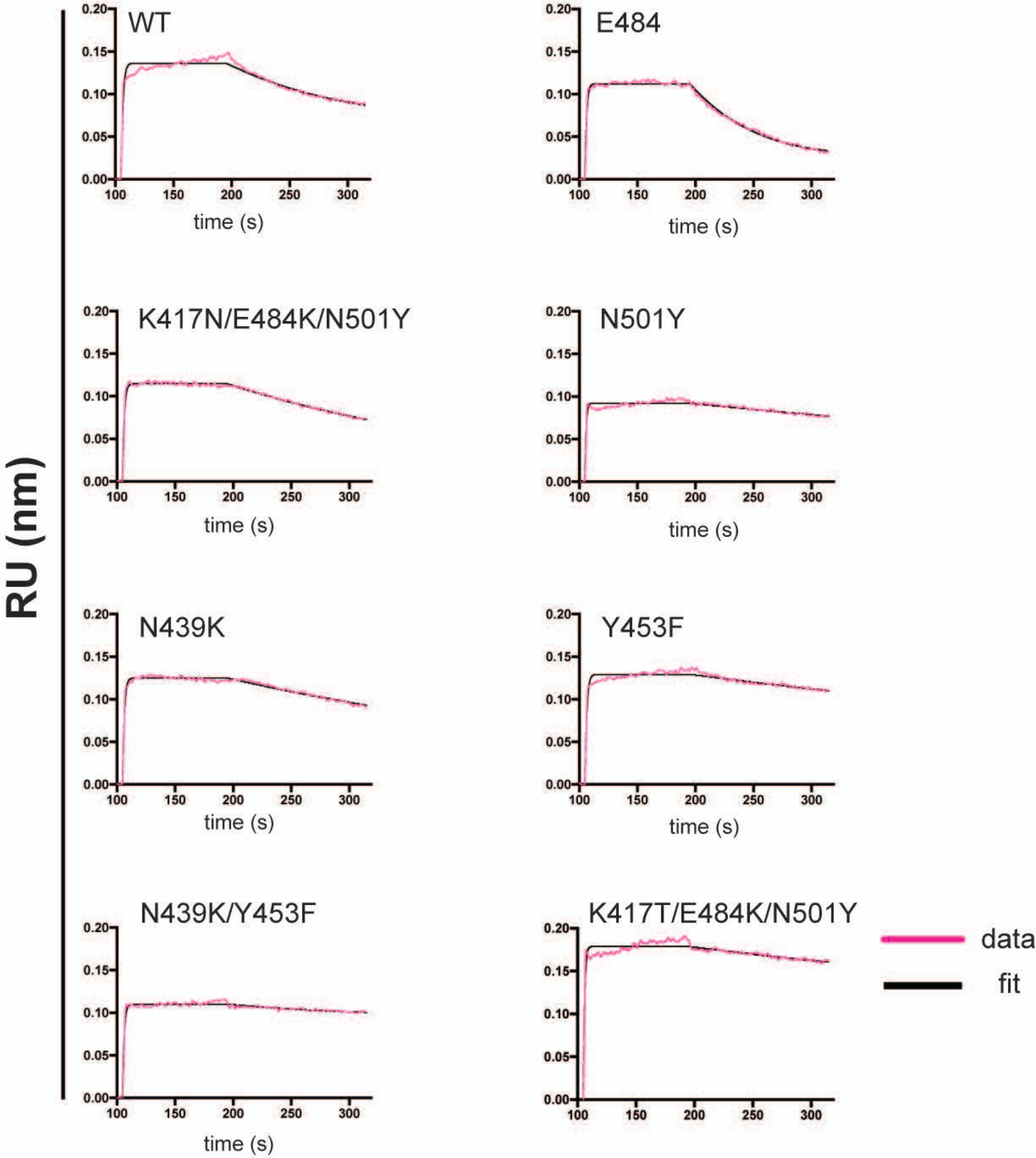
RU (nm)
WT
E484
K417N/E484K/N501Y
N501Y
N439K
Y453F
N439K/Y453F
K417T/E484K/N501Y
0.20
0.15
0.10
0.05
0.00
100
150
200
250
300
time (s)
data
fit

A

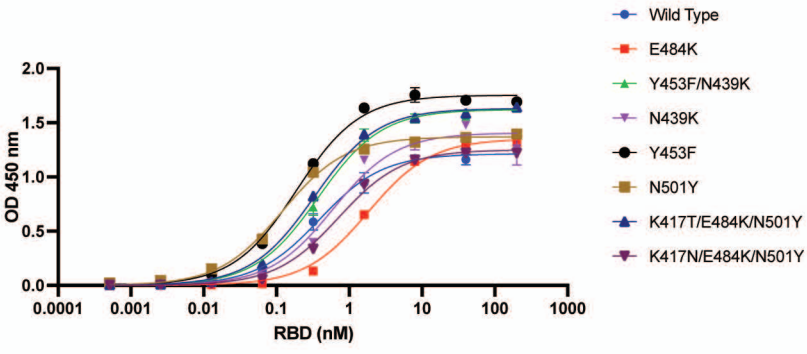

B

RBD variant	$K_D(10^{-11}M)$	Fold change
wild-type	38.8±0.5	1
N501Y	12±0.1	0.3
Y453F	18.9±0.1	0.5
N439K	59.8±9.3	1.5
Y453F/N439K	37.4±0.3	1
E484K	181.9±14.5	4.7
K417N/E484K/N501Y	71.3±3.7	1.8
K417T/E484K/N501Y	32.9±1.3	0.8